Modeling and Optimization of Vehicular-Enhanced Urban RANs with In-Band Backhaul

Laura Finarelli *Student Member, IEEE*, Falko Dressler *Fellow, IEEE*, Marco Ajmone Marsan *Life Fellow, IEEE*, Gianluca Rizzo *Senior Member, IEEE*

***Abstract*—Ground and aerial vehicles offer interesting opportunities for the dynamic deployment of small cell base stations (BSs) to complement static BS infrastructure in Beyond-5G and 6G networks. This enables a form of adaptive network densification that holds the potential to decrease infrastructure and operational costs. While previous studies provide insights into the feasibility of vehicular-enhanced RANs, they largely overlook the issue of determining in which conditions such adaptive densification provides a more efficient alternative to fully static (and often overprovisioned) deployments, particularly when accounting for the resource cost of wireless backhauling. The present work addresses this problem by proposing an analytical framework based on stochastic geometry to model vehicular-enhanced RANs that integrate static BSs with moving small cell BSs with in-band integrated access and backhaul. Our framework enables the assessment of the resource gains achievable through optimal provisioning of vehicular-enhanced RANs, via a joint optimization (in terms of capital expenditure and consumed energy) of deployment and resource allocation under QoS constraints, while accounting for road-grid mobility patterns and the complex interactions between access and backhaul links. Numerical assessment shows that our approach provides novel key insights on the conditions under which the dynamic network densification enabled by vehicle-based base stations can significantly reduce both operational and capital RAN costs.**

***Index Terms*—Moving networks, vehicular base stations, integrated access and backhaul, stochastic geometry, network densification, 6G.**

I. Introduction

Future cellular communications, such as 6G, will rely on a diverse set of network features to achieve unprecedented quality standards in data throughput and support for real-time services while also exploring sub-THz and THz communications [1]. Per-unit-area data traffic in these networks is projected to increase by roughly three orders of magnitude compared to current 5G deployments [2]. Future architectures should thus be designed to simultaneously absorb this surge in demand and support novel ultra–high-throughput services, including holographic communications [3] and immersive virtual reality [4]. Moreover, network traffic will exhibit a temporal variability and burstiness larger than in 5G due to the coexistence of sporadic bandwidth-intensive, event-driven immersive services with continuous, low-rate IoT traffic, under more heterogeneous QoS constraints [5], [6]. These traffic characteristics imply that a massive network densification will be required to provide the capacity and coverage needed by the new services, with 6G site densities potentially reaching more than $1000\ BSs/km^2$ in urban hotspots [7].

Densification imposes a double burden on operators, dramatically increasing both capital expenditures (CAPEX) to deploy more sites and operational expenditures (OPEX) for maintenance and power consumption of the enlarged set of network devices (mainly base stations). Indeed, infrastructure requirements grow superlinearly with peak demand due to traffic burstiness [8], [9]. This leads to very low average utilization rates of network infrastructures, particularly during off-peak times [10], [11].

To mitigate these resource inefficiencies and decrease the need for pervasive network densification, a promising avenue lies in the integration of vehicles in the RAN as mobile base stations [12], [13]. The use of small cells mounted on vehicles or other mobile platforms enables dynamic resource deployments, providing additional capacity exactly where and when needed, thus catering to localized traffic surges. This implementation of adaptive network densification, known as the *moving networks* (MNs) paradigm [14], potentially reduces the need for over-provisioning, but also the network operational expenditure, such as the energy required to operate the network. Recent studies underscore the potential of moving BSs. [15] shows that UAV-mounted BSs, when integrated with existing infrastructure and moved to demand hotspots, improve service continuity and network energy efficiency compared to static small cells. [13] shows that in some settings, a single mobile UAV unit can provide better coverage than five static small cells under realistic battery constraints.

Both aerial and ground unmanned vehicles have been proposed for temporary coverage in emergency scenarios or traffic hotspots [16], [17]. However, *natural MNs*, where vehicles are not controlled by the mobile network operator, but they are part of the pool of ground vehicles that traverse a given urban scenario every day [9], present the distinct

Copyright (c) 20xx IEEE. Personal use of this material is permitted. However, permission to use this material for any other purposes must be obtained from the IEEE by sending a request to pubs-permissions@ieee.org.

L. Finarelli is with HES-SO Valais, Switzerland, and TU Berlin, Germany, e-mail: laura.finarelli@hevs.ch.

M. Ajmone Marsan is with IMDEA Networks, Spain, e-mail: marco.ajmone@imdea.org.

F. Dressler is with TU Berlin, Germany, e-mail: dressler@ccs-labs.org.

G. Rizzo is with Università degli Studi di Torino, Dipartimento di Informatica, Italy, and HES-SO Valais, Switzerland, e-mail: gianluca.rizzo@unito.it, gianluca.rizzo@hevs.ch.

This work was supported by the DyMoNet project, jointly funded under the DFG–SNSF Lead Agency scheme by the German Research Foundation (DFG) under grant DR 639/25-1 and by the Swiss National Science Foundation (SNSF) under grant No. 201902. It was also partially supported by the UNITY-6G project, co-funded by the European Union's Horizon Europe Smart Networks and Services Joint Undertaking (SNS JU) research and innovation programme under Grant Agreement No. 101192650, and by the Swiss State Secretariat for Education, Research and Innovation (SERI).

advantage of being naturally distributed according to existing patterns of user densification. As such, they offer more practical and cost-effective temporary deployments, without requiring steering and active mobility control [18], [19]. Preliminary studies on the correlation between spatiotemporal patterns of vehicular traffic and of mobile users in urban settings [19], [20] provide solid empirical support for the feasibility of leveraging the uncontrolled patterns of everyday ground vehicles (e.g., private cars during commutes) to enable dynamic network densification in urban settings. This paradigm implies lower management complexity (as it does not require active driving and steering logic) and lower CAPEX, as it does not require an ad-hoc vehicle fleet. Recent research has so far focused on several technical issues brought about by the MN paradigm, such as interference mitigation, link stability, and handover management [21]–[24].

However, despite the potential resource efficiency gains being among the main drivers behind the interest in MNs, no work to date has investigated and characterized these gains as a function of the main system parameters. This is a key issue also because it is to date unclear if and in which cases the resource costs of the MN paradigm, due to wireless backhauling for the moving BSs and the performance impairments it brings about, outweigh its benefits in terms of resource efficiency with respect to purely static deployments, and which factors (e.g., relative CAPEX–OPEX balance) make MN-based architectures preferable to conventional deployments without moving base stations.

The present work represents a first attempt at addressing this issue. We propose a novel analytical framework for deriving a first-order characterization of the resource savings achievable via natural MNs. The goal is to determine the optimal configuration in terms of static and mobile BS densities that minimizes the overall resource requirements (and the network CAPEX and OPEX) while guaranteeing a target Quality of Service (QoS) for users at any point in time. Crucially, our approach accounts for the impact of wireless backhaul links on overall resource utilization and on target user-perceived QoS. We focus on Integrated Access and Backhaul (IAB) scenarios [25]. Indeed, given the severe spectrum pressure brought about by densification and Tbps-class services in 6G [26], sharing radio resources between access and backhaul is key to improving spatial spectrum reuse. However, our framework can be easily adapted to other backhaul technologies, and to a combination of them. Our main contributions are:

- We propose an analytical approach based on stochastic geometry for modeling the user-perceived performance in urban RANs with moving BSs, accounting for the impact of IAB and the effect of road-grid constrained mobility of moving BSs.
- We develop an optimization framework that derives, for a given spatio-temporal pattern of user demand, the optimal network configuration (in terms of installed BSs in all regions, and of active BSs at every time interval in each region) minimizing the network Total Cost of Ownership (i.e., a given combination of CAPEX and OPEX), subject to target user-perceived QoS constraints.
- We characterize the configurations resulting from our framework in different scenarios, performing a first evaluation of those conditions in which the MN paradigm enables substantial resource savings.
- We assess the impact of in-band backhauling on the overall efficiency of the MN paradigm by comparing it against out-of-band LEO satellite backhauling, that does not imply the same resource limitations of IAB.

The paper is structured as follows. Section II reviews the state of the art, Section III presents the system model and key assumptions, and Section IV derives the analytical framework. Section V formulates the optimization problems, solved and validated through numerical simulations in Section VI. Finally, Section VII concludes the paper.

II. Related Works

The deployment of base stations on vehicles has recently come into the spotlight, due to their ability to enable flexible deployments, dynamic coverage adaptation, improved spectrum and resource utilization, and efficient support for highly dynamic traffic conditions [27]–[29].

However, the MN paradigm brings several challenges related to mobility, interference management, wireless backhauling, and optimal dynamic network management, among others. As a result, the efficient design and operation of moving networks is currently an active area of research [12], [21]–[24], [24], [30]–[37]. Given the issues on interference management and handovers brought about by BS mobility, some works have focused on proactive interference mitigation through mobility prediction [23], on mechanisms for dynamic interference coordination in ultra-dense deployments [22], [24], on handover management approaches in highly dynamic vehicular environments [12], [38], and on techniques to enhance robustness against Doppler effects, blockage, and penetration losses in mmWave and high-speed communication scenarios [30], [39]. In particular, the combination of dense small-cell deployments, directional mmWave communications, and high vehicular mobility significantly increases handover frequency, beam management complexity, and link instability, making mobility-aware resource management a central research issue [38], [40]. In contrast to the above works, which primarily address link-level robustness and protocol mechanisms for interference and mobility management, our study focuses on the network-level efficiency trade-offs of vehicular densification, quantifying how moving base stations impact network CAPEX/OPEX for a target user-level QoS, under given traffic patterns.

In the present paper, we focus on moving networks with in-band integrated access and backhaul (IAB), in which spectrum sharing between access and backhaul links directly impacts the overall resource efficiency, scalability, and energy consumption of the MN paradigm [21], [30]. In these configurations, the interference between access and backhaul, along with mobility-induced path-loss variations, may significantly degrade link reliability, especially at mmWave frequencies [30]. Moreover, dynamic interference arising from unplanned MBS layouts induced by mobility leads to time-varying inter-BS patterns that degrade SINR for users and backhaul [22]–[24]. Our framework explicitly captures the complex access-backhaul

interactions and resource consumption of IAB. We formally model how macro BSs must split radio resources between ground user equipment (UEs) and backhaul links, introducing the backhaul violation probability to guarantee end-to-end QoS.

While terrestrial IAB introduces a strict coupling between access and backhaul resources, an emerging alternative for moving networks is the use of Non-Terrestrial Networks (NTN), such as Low Earth Orbit (LEO) satellite backhauling [41], [42]. Recent evaluations highlight that while LEO backhauling mitigates terrestrial spectrum sharing by offloading backhaul traffic to satellite bands, it introduces distinct challenges related to dynamic handovers and propagation delays [43]. In this paper, rather than modeling satellite link dynamics, we leverage the structural properties of an unconstrained, decoupled backhaul, typical of an ideal satellite or out-of-band link, as a fundamental baseline. This allows us to systematically isolate and quantify the exact capacity degradation and resource-splitting penalties unique to terrestrial in-band IAB deployments.

Among the open research issues related to the MN paradigm, the characterization of the potential gains in terms of resource efficiency brought about by such a paradigm is critical, as its supposed efficiency gains are, together with the natural adaptation to user density, among the main drivers of MNs. Despite that, however, to the best of our knowledge, no work to date has investigated and characterized these potential gains in natural MNs as a function of the main system parameters. The present paper addresses this gap in the state of the art by proposing an analytical approach based on stochastic geometry for modeling the performance of natural MNs in terms of resource efficiency, accounting for the impact of IAB and the effect of road grids, to identify when vehicular-enhanced deployments become more efficient than purely static ones.

Much of the analytical approaches to performance evaluation of cellular networks with moving elements is based on Stochastic Geometry (SG), as it allows deriving tractable closed-form expressions for several performance indicators of the network [44]. Several of these works adopt Poisson-Cox models of road-constrained layouts, such as those of roadside units or of relays mounted on vehicles, for a more realistic characterization of coverage probability and other key metrics of the network [28], [32], [33], [45]. However, (moving) relays typically operate under the scheduling control of a donor base station, often at the MAC or physical layer. In contrast, in the present work, the moving network elements we consider in MNs function as autonomous nodes with independent scheduling capabilities. This choice is key to exposing the impact of vehicular densification and in-band IAB backhauling on cell selection, interference, and the CAPEX/OPEX trade-offs between static and moving infrastructure at the network level.

Moreover, existing works focus primarily on link-level reliability and signal reach [46]. In the present work, instead, we aim to evaluate the efficiency trade-offs between fully static infrastructure and hybrid moving/static scenarios, while guaranteeing a given level of the QoS perceived by the user. Thus, our work focuses on how moving base stations with independent scheduling and in-band backhauling affect the overall system capacity and the resource efficiency of the network.

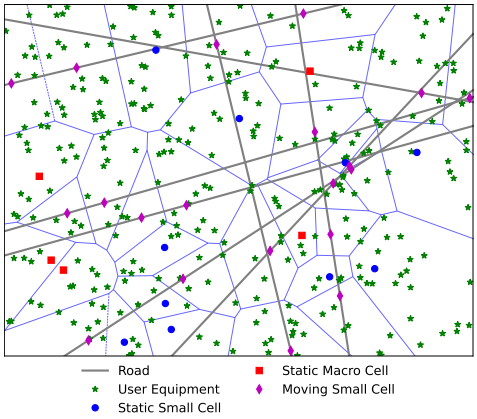


Figure 1. A sample realization of the network at a specific time instant, with the three BS tiers and same trx powers. The grey lines are part of the PCLP, and they model the road grid on which moving BSs are located.

Most existing performance analyses of IAB via SG focus on link-level feasibility or coverage probability, in static scenarios [37], [47]. The present work advances the state of the art by explicitly modeling the resource coupling induced by IAB in an MN as a functional constraint within the optimization framework. Unlike prior works focusing primarily on coverage probability or positioning, our framework introduces a novel optimization problem that jointly optimizes the spatial densities of *both static and moving BSs* under strict QoS constraints. Furthermore, we provide a Total Cost of Ownership (TCO) analysis that combines CAPEX and load-proportional OPEX energy models, demonstrating the explicit conditions under which natural moving networks yield substantial resource savings over traditional, overprovisioned static infrastructures. This paper extends the analytical framework developed in [31] with a three-tier architecture that incorporates PCLP distributed moving BSs, and by applying the resulting methodology to an idealized LEO backhaul setting. In addition, the work generalizes the associated optimization framework to include TCO minimization under vehicular traffic flows and active BS density control (Sec. V), provides an energy-optimal performance analysis, and presents a comparative assessment against LEO backhaul scenarios (Sec. VI).

III. System Model

We consider a region of the plane modeling an urban scenario. The network is composed of three tiers of base stations (BSs). A fraction of the BSs in the region, denoted as *moving BS*, are installed on vehicles, such as private or shared cars, and thus capable of moving within the region. They are small cell BSs, i.e., with a lower transmit power than macro BS. To account for the spatial features induced by the road grid, we assume that at any given time, moving BS are distributed according to a Poisson-Cox Line Process (PCLP) Ξ within the region [28]. A PCLP is a PPP restricted to an isotropic planar line process Φ_l, of intensity λ_l.

The remaining BSs do not change their location over time. They consist of macro BSs, typically installed on buildings or tall structures, and microcell/small cell BSs, often installed on light poles. Each of these two classes of BSs is distributed

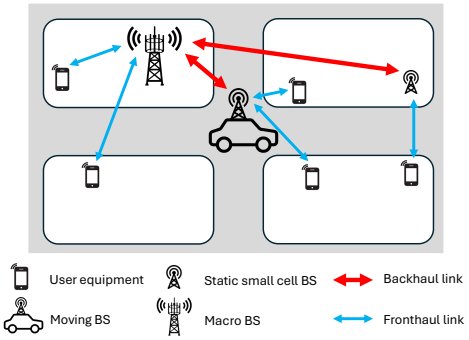


Figure 2. Illustration of the considered network scenario with IAB, with the three tiers of BSs. Macro BSs serve UEs and act as access points for small cells' backhaul links.

according to an (independent) homogeneous planar Poisson Point Process (PPP), denoted with Φ_M and Φ_s respectively, and with spatial intensity λ_M and λ_s. The PPP assumption is adopted for analytical tractability. A first assessment of the sensitivity of the results to a more regular, repulsive layout of macro BSs, modeled as an $\alpha-$Ginibre point process, is reported in Section VI-A. Fig. 1 shows a sample realization of these point processes.

Such a scenario models a *multi-tier densified RAN*, where macro BSs provide a blanket coverage, and small cells reduce dead zones, coverage holes, and help increase capacity. As for the backhauling technologies, we consider two different scenarios. In the Integrated Access and Backhaul (IAB) scenario, the same wireless spectrum and infrastructure are used both to provide access to user devices and to backhaul traffic between moving and static small cell BS and the core network. In this scenario, macro BSs also act as wireless access points for the other two classes of BSs. In the second scenario, out-of-band backhauling is employed. Specifically, we assume that both static small cell BSs and Moving BSs use LEO satellite links for their backhaul traffic.

We assume that user equipments (UEs) (which model, e.g., broadband terminals, or IoT devices,) are distributed in space according to a PPP. Fig. 2 illustrates the considered system. We consider the region to be divided into Z different *areas*. With λ_u^z we denote the intensity of the PPP of UEs, measured in users per m^2. We adopt a simple channel model that accounts only for distance-dependent path loss. Note, however, that our model can be extended to accommodate more realistic propagation models, and account for fading as well as beamforming, at the cost of more complex analytical expressions. We consider only the downlink of the cellular access network, and we assume that the generic UE, located at x is served by the BS that provides the largest SINR at x. Similarly, for wireless backhaul links, the small cell BS (static or moving) at x is served by the macro BS delivering the largest SINR at x. Leveraging Shannon's capacity law, the capacity of a user located at a distance r from the BS is

$$C(r,P,I) = B\log_2(1+Pr^{-\alpha}(N_0+I(r))^{-1})$$

where P is the BS transmit power, B the channel bandwidth, α the attenuation coefficient, I the total received interfering power, and N_0 is the power spectral density of the additive white Gaussian noise.

Table I
MAIN NOTATION USED IN THE PAPER.

Notation	Parameter
λ_u^z	Intensity of the PPP of UEs in the $z-th$ area (m^{-2})
λ_s^z	Intensity of the PPP of static small cells in the $z-th$ area (m^{-2})
λ_M^z	Intensity of the PPP of static macro cells in the $z-th$ area (m^{-2})
λ_m^z	Intensity of the Poisson-Cox point process of moving BSs in the $z-th$ area and time slot j (m^{-2})
λ_l	Line density of the PCLP of moving BSs (m^{-1})
τ_0	Target per-bit delay (s)

We assume that a weighted processor-sharing (WPS) mechanism is used to divide the BS time among all the connected users. By doing so, a notion of fairness is imposed among users from the same class and associated with the same BS, since they are all served for an identical fraction of time. We model wireless in-band backhauling by assuming that macro BSs serve two classes of *users* (UEs, and small cells), each with its own WPS weight. To model the QoS perceived by a user from these classes, we use the *per-bit delay*, defined as the inverse of the short-term user throughput [48]. We assume that the mean utilization of BS (i.e., the fraction of time during which a BS, mobile or static, is active) and the WPS weights are tuned in such a way as to achieve the target QoS for all classes of users.

In the IAB scenario, we assume that at each macro BS, the WPS weights for users and for the backhaul (BH) link for small cells are respectively equal to $\phi^z \geq 0$ and to one, with ϕ^z taking the same value for all UEs.

We assumed that the frequencies used by backhaul links from the donor to the moving cell are those used by the macro BS to serve users associated with them in the downlink. The frequencies used by moving BSs to serve users associated with them in the downlink are also used for the uplink of the backhaul connection, i.e., from the moving BS to the donor macro BS. We assumed no frequency reuse, though random frequency reuse can be easily introduced in our analytical framework.

The utilization of a base station is the fraction of the base station time spent serving users. For a macro BS serving N_s static small cell BSs, N_m moving small cell BSs and N_U UEs, in the z-th area, the utilization is thus

$$U_M^z = \frac{\phi^z N_U + N_s + N_m}{\phi^z N_U + N_s + N_m + \beta_M}$$

where β_M is the fraction of BS time during which the macro cell BS is not serving any user (and thus potentially saving energy). For a small cell BS (static or moving) serving N_U users, instead, we have

$$U_j^z = N_U/(N_U+\beta_j)$$

with β_j, $j \in \{m,s\}$ modeling the moving (resp. static) BS idle time. In the LEO backhauling scenario, instead, macro cell BSs have only fronthaul wireless traffic. Thus, the expressions for the utilization are derived from the previous ones, by setting $\phi^z = 1$, and $N_s,\ N_m = 0$.

For UEs, the key performance parameter is the Palm expectation of the per-bit delay experienced by a typical user who is just beginning service [49]. For backhauling links instead, the main performance indicator is the *violation*

probability, i.e., the probability that the per-bit delay perceived by the backhauling connection is insufficient to carry the aggregate traffic demand.

Thus, both macro and micro BSs tune their utilization and the WPS weight to have both the Palm expectation of the per-bit delay perceived by the typical BB user coinciding with a target value τ_0, and the violation probability for BH traffic below a target value δ.

The power consumption of static BSs (both macro and small), which is drawn from the power grid, is modeled as:

$$E_s(U,P) = q_1 + U(q_2 + q_3 P) \tag{1}$$

where U is the BS utilization. q_1 accounts for the part of the consumed power which is independent of the traffic load or the transmit power, and it is thus the power consumed when the BS is idle. q_2 and q_3 instead model the power consumption associated with the computational and cooling processes, proportional to the utilization and power consumed during signal transmission, which depends both on U and P.

For the power consumption of moving BSs, we introduce the factor $\iota \in (0,1]$ modeling the battery efficiency. Thus, the power consumed by a moving BS is given by $E_m(U,P) = E_s(U,P)/\iota$.

IV. Modeling User Perceived Performance

In this section, we derive analytical relationships between the main system parameters and the network's key performance indicators. To this end, we consider the *ideal per-bit delay* experienced by a user, defined as the per-bit delay measured when the serving BS operates at full utilization, i.e., when its utilization equals 1. Indeed, given our assumptions, the actual per-bit delay experienced by a user is given by the product of the ideal per-bit delay and the BS utilization. In what follows, we focus on the IAB scenario, as the expressions for the LEO backhauling case can be easily derived from those of the former.

Let $S(x)$ denote the location of the BS that is closest to the user located at x. For the typical user at the origin served by the closest static macro BS in $S(0)$[1], the ideal per-bit delay perceived in area z is

$$\tau_M^z(S(0)) = \frac{N_s(S(0)) + N_m(S(0)) + \phi^z N_U(S(0))}{\phi^z C(D(0), P_M, I)} \tag{2}$$

where N_m, N_s, and N_U are the number of moving, static small cell BSs, and UEs served by the static macro cell BS in $S(0)$ respectively, P_M is the macro BS transmit power, and $D(0)$ is the distance between the user at the origin and its serving BS.

For the downlink of a wireless backhauling link (i.e., from the serving macro BS to the served BS, located at the origin), the ideal per-bit delay is

$$\tau_{BH}^z(S(0)) = \tau_M^z(S(0))\phi^z$$

Likewise, the ideal per-bit delay for a moving (resp. static) small cell user is

$$\tau_j^z(S(0)) = \frac{N_U(S(0))}{C(D(0), P_S, I)}, \quad j \in \{m, s\} \tag{3}$$

[1]We recall that under the Palm probability, we can always assume there exists a typical user located at the origin.

where P_S is the transmit power of small cells, N_U is the number of UEs served by the macro (resp. the static small cell) in $S(0)$, and $D(0)$ is the distance between the typical user and its serving small cell.

In the z-th area, let $\bar{\tau}_M^z, \bar{\tau}_m^z$ and $\bar{\tau}_s^z$ denote the Palm expectation of the ideal per-bit delays perceived by BB users joining the system, and let $\bar{\boldsymbol{\tau}}^{\boldsymbol{z}} = (\bar{\tau}_M^z, \bar{\tau}_m^z, \bar{\tau}_s^z)$. With λ_M^z, λ_s^z, and λ_m^z, we denote the mean density of macro, static small, and the linear density of moving BSs, respectively, and let $\boldsymbol{\lambda}^z = (\lambda_M^z, \lambda_s^z, \lambda_m^z)$. The following result connects the mean total interference experienced by a user with the mean ideal per-bit delay perceived by users within the system.

Lemma 1. *The mean interference power received by a user in z associated with a macro BS is*

$$\bar{I}_M(r, \bar{\boldsymbol{\tau}}^{\boldsymbol{z}}) = \frac{2\pi r^{2-\alpha}}{(\alpha-2)} P_M \lambda_M^z \min\left(\frac{\bar{\tau}_M}{\tau_0}, 1\right)$$

The mean interference power received by a user in z associated with a small cell (static or moving) is

$$\bar{I}_S(r, \bar{\boldsymbol{\tau}}^{\boldsymbol{z}}) = \frac{2\pi r^{2-\alpha}}{(\alpha-2)} P_S \left[\lambda_s^z \min\left(\frac{\bar{\tau}_s}{\tau_0}, 1\right) + \pi\lambda_l \lambda_m^z \min\left(\frac{\bar{\tau}_m}{\tau_0}, 1\right)\right]$$

For the proof, please refer to Appendix A.

This result considers that the PPP of interfering BSs is the weighted superposition of the processes from the three tiers. We now derive the Palm probability distribution function (PDF) of the distance between the typical user located at the origin and its serving BS.

Theorem 1. *The PDF of the distance from the origin to the closest BS in the $z-$th area under the Palm distribution of Φ_u is*

$$f_R^z(r) = e^{-\pi r^2(\lambda_M^z + \lambda_s^z \rho^2) - 2\lambda_l \pi \int_0^{\rho r}(1 - e^{-2\lambda_m^z \sqrt{(\rho r)^2 - u^2}})du} \cdot \left[2\pi r(\lambda_M^z + \lambda_s^z \rho^2) + \int_0^{\rho r} \frac{4\pi\lambda_l \lambda_m^z \rho^2 r e^{-2\lambda_m^z \sqrt{(\rho r)^2 - u^2}}}{\sqrt{(\rho r)^2 - u^2}} du\right] \tag{4}$$

with $\rho = \sqrt[\alpha]{\frac{P_S}{P_M}}$.

The proof can be found in Appendix B. The derivation of this result exploits the fact that macro and small cells transmit at different power levels and follow distinct spatial point processes. These two factors jointly determine their respective coverage radii and, consequently, the typical size of their Voronoi cells.

The following theorem gives the expressions for the Palm expectation of the ideal per-bit delays perceived by users.

Theorem 2. *In the IAB scenario, the Palm expectation of the ideal per-bit delay perceived by users joining the system in area z, and served by a macro (respectively, a static small and a moving small) cell BS is approximated as the unique solution of the following fixed point problems:*

$$\begin{aligned} \bar{\tau}_M^z &= \int_0^\infty \left(\phi^z \lambda_u^z h_M^z(r) + (\lambda_m^z \pi\lambda_l + \lambda_s^z) h_{BH}^z(r)\right) \cdot \\ &\quad \cdot \frac{f_R^z(r)}{C(r, P_M, I(r, \bar{\boldsymbol{\tau}}^{\boldsymbol{z}}))\phi^z} dr \\ \bar{\tau}_m^z &= \bar{\tau}_s^z = \int_0^\infty \lambda_u^z h_S^z(r) \frac{f_R^z(r)}{C(r, P_S, I(r, \bar{\boldsymbol{\tau}}^{\boldsymbol{z}}))} dr \end{aligned} \tag{5}$$

$$h_S^z(r) = \int_0^\infty \int_0^{2\pi} e^{-\lambda_M^z A(r,x/\rho,\theta) - \lambda_s^z A(r,x,\theta)} e^{-2\lambda_l \pi \int_0^{r_A(1)} (1-\exp(-2\lambda_m^z \sqrt{r_A(1)^2-u^2}) du} x d\theta dx$$

$$h_M^z(r) = \int_0^\infty \int_0^{2\pi} e^{-\lambda_M^z A(r,x,\theta) - \lambda_s^z A(r,\rho x,\theta)} e^{-2\lambda_l \pi \int_0^{r_A(\rho)} (1-\exp(-2\lambda_m^z \sqrt{r_A(\rho)^2-u^2}) du} x d\theta dx \quad (6)$$

$$h_{BH}^z(r) = \int_0^\infty \int_0^{2\pi} e^{-\lambda_M^z A(r,x,\theta)} x d\theta dx$$

with $A(r,x,\theta) = \pi x^2 - \left[r^2 \arccos\left(\frac{r+x\sin(\theta)}{d(r,x,\theta)}\right) + x^2 \arccos\left(\frac{x+r\sin(\theta)}{d(r,x,\theta)}\right) - \frac{1}{2}\sqrt{[r^2-(d(r,x,\theta)-x)^2][(d(r,x,\theta)+x)^2-r^2]} \right]$ *and* $r_A(z) = \sqrt{\frac{A(r,zx,\theta)}{\pi}}$. *$d(r,x,\theta)$ denotes the euclidean distance between (x,θ) and $(0,-r)$.*

In the LEO backhauling scenario, Equation 5 becomes

$$\bar{\tau}_M^z = \int_0^\infty \lambda_u^z h_M(r) \frac{f_R^z(r)}{C(r, P_M, I(r, \bar{\boldsymbol{\tau}}^{\boldsymbol{z}}))\phi^z} dr$$

while all other expressions remain unaltered.

The proof, which can be found in can be found in Appendix C, revolves around the characterization of the statistics of the area of the Voronoi cells, which allows modeling the service load on static and moving BSs.

In the IAB case, let τ_{BH}^z denote the ideal per-bit delay at the backhauling link in area z, which a macro BS delivers to a moving (or a static) small cell BS in downlink. The following result provides the expressions for the cumulative distribution function (CDF) of these parameters.

Lemma 2. *In the IAB scenario, the cumulative distribution function of τ_{BH} in a given area z, is*

$$CDF_{\tau_{BH}^z}(\tau) = CDF_r\Big((g^z)^{-1}(\tau)\Big)$$

where

$$CDF_r(y) = \int_0^y e^{-\lambda_M^z \pi x^2} \lambda_M^z 2\pi x dx$$

$$g^z(r) = \frac{(\lambda_s^z + \pi\lambda_l\lambda_m^z) h_{BH}^z(r) + \phi^z \lambda_u^z h_M^z(r)}{C(r, P_M, I(r,\bar{\tau}))}$$

and $h_M^z(r)$, $h_{BH}^z(r)$ are given by Theorem 2

For the proof, please refer to Appendix D. Note that the expression for the BH per-bit delay as a function of r can be derived from Eq. 2.

In the IAB scenario, to model the violation probability of a BH link, we focus on the traffic demand at a small cell (static or moving), in terms of the per-bit delay of the aggregate downlink traffic at the given small cell BS. The violation probability is then the probability that the per-bit delay perceived in downlink by moving (or static small) BSs is larger than the aggregate traffic demand in downlink of a moving (or a static small) BS.

Theorem 3. *In the IAB scenario, for a small cell (moving or static) the BH violation probability in area z is*

$$V^z = \int_0^\infty f_{\tau_d}(x)\left(1 - CDF_{\tau_{BH}}^z\left(\bar{U}_M^z\, x\right)\right) dx$$

with

$$f_{\tau_d}(t) = a^{\frac{7}{2}} \frac{343}{15} \sqrt{\frac{7}{2\pi}} t^{-\frac{9}{2}} e^{-\frac{7}{2}\frac{a}{t}}$$

and $a = \frac{\tau_0}{\lambda_u^z}(\lambda_M^z + \rho\lambda_m^z\lambda_l\pi + \rho\lambda_s^z)$

For the proof, please refer to Appendix E. The result is based on the formula of the mean area of a Voronoi cell in a Poisson point process, which is related to the average number of users served by small cells. We remark that all these results have been derived while neglecting border effects, such as those due to BSs serving users from two or more different areas. Thus, they hold greater accuracy the farther the user is from the borders of the given area[2].

V. Optimal dimensioning of a moving network

One of the key drivers of the moving network paradigm is its potential to decrease the number of required BSs and reduce overall energy consumption, while still ensuring that users across the target region receive the expected quality of service.

To quantify such potential, in this section, we propose an optimization framework for QoS-aware optimal dimensioning of a RAN with moving small cell BSs. We consider that for the given geographical region (ideally comprising an urban region and its immediate surroundings) the spatiotemporal patterns of user densities across a given (finite) time window are known (or predictable with reasonable accuracy). As these patterns typically exhibit periodicity over time (in terms of days, weeks, or months), a suitable time window may be chosen as an integer multiple of the period characterizing these variations.

We consider the time window to be divided into a set of J intervals of duration Δ_j, and let j be the label of the $j-th$ interval. Thus, user density in area z at time slot j is denoted as $\lambda_{u,j}^z$. This may model the effects of day/night activity patterns, of commuting, and other factors affecting spatio-temporal patterns of user distribution.

In every area, and for every class $i \in \{M, m, s\}$ of BSs, with $\hat{\lambda}_i^z$ we denote the density of *deployed* BSs (either in a fixed geographical location, or installed on vehicles). For each of these populations of BSs, at each time slot j with $\lambda_{i,j}^z$ we denote the density of BS subpopulations that are *active* at time j, i.e., that are not in standby or off mode and thus actively serving users.

Moreover, we assume that the vehicles hosting BSs follow their inherent mobility patterns (e.g., commuting routes or service operations) and cannot be actively steered to optimize network performance. Their mobility patterns thus impose an additional design constraint on the network, as they limit the availability of moving BS in each area at a given time slot. Specifically, for the number of vehicles in area z and time j, the following balance equation holds:

$$\eta_{m,j+1}^z = \eta_{m,j}^z + \sum_{k\in\mathcal{Z}} \left(\eta_{m,j}^{k\to z} - \eta_{m,j}^{z\to k}\right) + s_j^z$$

Where $\eta_{m,j}^z$ is the total amount of vehicles in area z at time j, $\sum_{k\in\mathcal{Z}} \eta_{m,j}^{z\to k}$ are the vehicles leaving the area at time j,

[2]Note that the impact of fast fading and Doppler can be accommodated by introducing a fading margin to the backhaul per-bit delay threshold. In a similar way, we can account for the impact of non-payload signaling on backhaul links.

$\sum_{k\in\mathcal{Z}} \eta_{m,j}^{k\to z}$ are those entering the area at j, and s_j^z are the exogenous net arrivals or departures of vehicles in area z at time j, modeling vehicles that start or end their trip at time j in area z. All these quantities are assumed to be derived from data about vehicular traffic flows in the considered region. Let $\hat{\lambda}_{m,j}^z = p_{BS,j}^z \eta_j^z$, where $p_{BS,j}^z$ express the fraction of vehicles in each area and time slot on which a BS has been installed, with $0 \le p_{BS,j}^z \le 1$. We have:

$$p_{BS,j+1}^z\, \eta_{m,j+1}^z = p_{BS,j}^z\, \eta_{m,j}^z + p_{BS,j}^z\, s_j^z + \\ + \sum_{k\in\mathcal{Z}} \left(p_{BS,j}^k\, \eta_{m,j}^{k\to z} - p_{BS,j}^z\, \eta_{m,j}^{z\to k}\right) \tag{7}$$

This framework can model a broad range of spatio-temporal variations in vehicular traffic and user density, and the correlations among them.

For the given region and time window, we thus formalize an optimization problem that aims at minimizing the RAN total cost of ownership (TCO). This metric combines the OPEX given mainly by the energy consumed (related to patterns of activity of BSs), and the CAPEX, which accounts for the cost of purchasing and deploying BSs. The minimization problem must guarantee that the desired QoS is met for both fronthaul and backhaul wireless transmissions, at any time slot and area of the region.

The optimization variables are the density of macro, static small, and moving BSs provisioned by the mobile operator, the density of active BSs for each category, and the values of the WPS weights ϕ_j^z, in each area at each time slot. The solution to such a problem thus determines the mobility strategies and the activation patterns for each class of BSs that achieve the optimal TCO for the network.

Problem 1. ***TCO-optimal configuration of a moving network (IAB scenario)***

$$\underset{\{\boldsymbol{\lambda_j^z}\},\{\hat{\boldsymbol{\lambda}}_{\boldsymbol{j}}^{\boldsymbol{z}}\},\{\phi_j^z\}}{\textit{minimize}} \quad \sum_j \Delta_j \sum_z \left[\lambda_{m,j}^z \lambda_l \pi E_m \left(\frac{\bar{\tau}_{m,j}}{\tau_0}\right) + \lambda_s^z E_s \left(\frac{\bar{\tau}_{s,j}}{\tau_0}\right) + \lambda_M^z E_s \left(\frac{\bar{\tau}_{M,j}}{\tau_0}\right)\right] A_z + \\ + \gamma A_z \left[\sum_z \hat{\lambda}_M^z + \left(\mu_m \max_j \sum_z \hat{\lambda}_{m,j}^z + \mu_s \sum_z \hat{\lambda}_s^z\right)\right]$$

Subject to, $\forall\, j, z$*:*

$$\textit{Constraint}\quad (7) \qquad \hat{\lambda}_{m,j}^z = p_{BS,j}^z \eta_{m,j}^z \quad (8) \qquad \bar{\tau}_{M,j}^z,\, \bar{\tau}_{s,j}^z,\, \bar{\tau}_{m,j}^z \le \tau_0 \quad (9)$$

$$V_j^z \le \delta \quad (10) \qquad \phi_j^z \ge 0 \quad (11) \qquad \lambda_{m,j}^z \lambda_l \pi \le \hat{\lambda}_{m,j}^z \quad (12) \qquad 0 \le p_{BS,j}^z \le 1 \quad (13)$$

The objective function in Problem 1 is the linear combination of the energy consumed by the network in the given region and the total cost of purchasing and deploying the BSs from the three categories.

The parameter γ is the *CAPEX/OPEX ratio*, and it models the relationship between one-time investment costs (e.g., purchasing and installing base stations) and recurring operational costs (e.g., energy expenses for running the base stations) in the network's life cycle. It is a function of typical CAPEX per base station type (purchase and installation), as well as the energy price per kWh, among others. A_z denotes the geographic size (in m^2) of the z-th area. Parameters $\mu_m, \mu_s \ge 0$ capture the relative difference in unitary cost (purchase, reuse, and deployment) between small moving/static BSs, respectively, and macro BSs. Note that typically $\mu_m < \mu_s < 1$. This reflects the usually higher bureaucratic, architectural, and regulatory expenditures involved in deploying macro infrastructure compared to the relatively lower costs of small cell BS deployments and the higher costs of static BS installations. However, it is important to consider that the mobility aspects might introduce additional operational costs or logistical complexities not fully captured by a single scalar cost ratio, which could affect μ_m in specific deployment scenarios.

Constraint 9 imposes that the target QoS for UEs is achieved in all base station classes. The backhaul violation probability threshold δ in constraint 10 controls the probability that a small cell's backhaul link cannot sustain the aggregate traffic demand. It must be set to a low enough value for violation events to have a negligible effect on the performance perceived by users.

Thus, Problem 1 gives not only the TCO-optimal densities of deployed BS for each of the three categories, but it also defines the TCO-optimal strategies for deploying the moving BSs among the vehicles that traverse the region over time, accounting for vehicular mobility patterns.

In the LEO backhauling scenario, the objective function should account for potential differences in costs between satellite and wired backhaul. In this scenario, the RAN TCO is minimized under the assumption that satellite backhauling always provides sufficient throughput, comparable to that of wired backhaul solutions. As a result, (similarly to wired backhauling for macro BSs), satellite backhaul link-quality and capacity limitations are not explicitly modeled in either the objective function or the constraints of the optimization problem. This allows isolating the impact of in-band backhauling costs in our analysis (Sec. VI), modeling LEO backhauling as a dedicated, unconstrained alternative despite real-world challenges like latency or handovers [50], [51]. We therefore have the following formulation:

Problem 2. ***TCO-optimal configuration (LEO backhaul scenario)***

$$\underset{\{\boldsymbol{\lambda_j^z}\},\{\hat{\boldsymbol{\lambda}}_{\boldsymbol{j}}^{\boldsymbol{z}}\}}{\textit{minimize}} \quad \sum_j \Delta_j \sum_z \left[\mu \lambda_{m,j}^z \lambda_l \pi E_m \left(\frac{\bar{\tau}_{m,j}}{\tau_0}\right) + \lambda_s^z E_s \left(\frac{\bar{\tau}_{s,j}}{\tau_0}\right) + \lambda_M^z E_s \left(\frac{\bar{\tau}_{M,j}}{\tau_0}\right)\right] A_z \\ + \gamma A_z \left[\sum_z \hat{\lambda}_M^z + \left(\mu_m \max_j \sum_z \hat{\lambda}_{m,j}^z + \mu_s \sum_z \hat{\lambda}_s^z\right)\right]$$

Subject to constraints (7), (8), (9), (12), (13).

In this formulation, μ models the energy cost of satellite backhauling in moving BSs.

Both problem formulations involve nonlinear and nonconvex constraints, which pose significant challenges for efficient optimization using exact methods. To address this, we adopt a heuristic approach based on the Hippopotamus Optimization Algorithm (HO) [52], which has demonstrated superior

performance on similar problem classes. HO is a three-phase metaheuristic that explores the solution space through iterative position updating, defensive strategies to avoid local optima, and evasion techniques to enhance diversification.

The non-convex inequality constraints are handled using an additive penalty function incorporated into the objective, which penalizes infeasible solutions to guide the search toward the feasible region. The primary hyperparameter of the algorithm is the number of agents, which represent candidate solutions to the optimization problem. Each agent's position in the search space corresponds to a specific set of decision variable values. Increasing the number of agents generally improves the algorithm's ability to explore the solution space and increases the likelihood of finding an optimal or near-optimal solution. In the next section, we analyze how this hyperparameter affects the performance of the heuristic.

VI. Numerical assessment

In this section, we validate our analytical framework through Monte Carlo simulations, assess the sensitivity of the results to the macro BS layout, and characterize optimal moving network configurations with respect to key system parameters.

We assume all BSs operate at a frequency of 1.5 GHz. The bandwidth is set to 100 MHz for macro cell BSs and 20 MHz for small cell BSs [53]. The target QoS for broadband users is set to a per-bit delay of 10^{-5} seconds, which corresponds to an average throughput of 100 kbps suitable for light browsing and video calls, and 10^{-6} seconds typical of video streaming, consistent with the Enhanced Mobile Broadband (eMBB) framework [54]. The model assumes a path-loss exponent of 3, typical for urban environments, with transmit powers $P_M = 10\,W$ for macro cell BSs and $P_S = 3\,W$ for small cell BSs. User densities vary from 10^{-4} to 10^{-1} users per m^2, reflecting typical daily variations in residential and business districts [55].

To analyze both current and prospective energy scenarios in cellular networks, we consider two distinct configurations for the BS energy model. In the first one, denoted as Low Load Proportionality (LLP), the amount of consumed power that depends on load is 35% of the total. To model more recent BS architectures, which achieve a higher level of load proportionality thanks to a combination of modular HW architecture and cloud-based aggregated processing [56], we considered the High Load Proportionality (HLP) configuration, in which 75% of the power consumption depends on traffic load. The parameters (q_1, q_2, q_3) of the BS energy model (Eq. 1) are $(1100, 100, 30)$ for LLP macro BSs, $(482.3, 17.69, 100)$ for HLP macro BSs, and $(330, 90, 10)$ for small-cell BSs. These parameter values have been derived based on maximum power ratings of 1500 W for macro BSs and 450 W for small cell BSs, as in [56]. Unless otherwise stated, the battery efficiency coefficient ι for moving BSs is set to 1. Unless otherwise stated, we assumed no upper bound to moving BS density (constraint 8).

The multiplicative factors employed in the penalty functions for solving Problems 1 and 2 were determined empirically. Specifically, the factor is set to 100 for Constraint 9 and to 150 for Constraint 10. The number of search agents in the HO algorithm was set to 70, as preliminary tests showed this value achieves an effective exploration-exploitation balance while maintaining computational tractability. As for the termination criterion for the HO algorithm, we assumed that the procedure stops either when the average change in the fitness function remains below 10^{-8} for 30 consecutive iterations, or when the standard deviation of the fitness values over the most recent 10 iterations falls below 10^{-6}. These threshold values were determined through preliminary numerical experiments to achieve an optimal balance between thorough exploration of the parameter space and computational tractability.

Table II
Model Validation: Analytical vs. Simulation Results for $\tau_0 = 10^{-5}$ s, $\lambda_u \in \{10^{-3}, 5 \cdot 10^{-3}, 10^{-2}\}$ users/m^2. The density of static small cells is zero across all setups.

User density [m^{-2}]		$1e{-3}$	$5e{-3}$	$1e{-2}$
Static macro density [m^{-2}]		$4.48e{-4}$	$7.90e{-4}$	$2.10e{-3}$
Moving small density [m^{-2}]		$2.20e{-3}$	$5.00e{-5}$	$1.00e{-4}$
Mean per-bit delay (Static macro) [μs]	Analysis	3.21	3.90	8.66
	Simulation	3.58	3.79	8.11
	95% Conf. Int.	[3.11, 4.05]	[3.65, 3.93]	[7.93, 9.39]
	Simulation (Ginibre $\alpha = 0.5$)	2.15	3.30	6.79
	95% Conf. Int.	[2.10, 2.20]	[3.19, 3.41]	[6.62, 6.96]
	Simulation (Ginibre $\alpha = 1$)	1.47	3.03	5.71
	95% Conf. Int.	[1.43, 1.51]	[2.95, 3.11]	[5.63, 5.79]
Mean per-bit delay (Moving small) [μs]	Analysis	4.82	5.47	5.11
	Simulation	4.76	4.98	4.61
	95% Conf. Int.	[4.62, 4.90]	[4.46, 5.50]	[4.51, 5.71]
	Simulation (Ginibre $\alpha = 0.5$)	3.22	3.69	3.19
	95% Conf. Int.	[3.17, 3.27]	[3.51, 3.87]	[2.98, 3.56]
	Simulation (Ginibre $\alpha = 1$)	1.57	2.49	2.14
	95%Conf. Int.	[1.54, 1.60]	[2.36, 2.62]	[1.97, 2.31]
Violation probability (Moving small)	Analysis	0.03	0.96	0.918
	Simulation	0	0.95	0.915
	95% Conf. Int.	[0, 0.05]	[0.95, 0.97]	[0.85, 0.96]

To assess the effectiveness of such a heuristic parameter selection process, we solved Problem 1 with our HO heuristic under two target per-bit delay values and for different energy models, for both $\gamma = \infty$ (CAPEX-only) and $\gamma = 0$ (OPEX-only) scenarios. To this end, we considered a simplified three-tier setting, composed of a single area and a single time slot (i.e., a static setup), with user density equal to 10^{-4} users per m^2. Fig. 3 shows how the value of the solution of Problem 1 derived via the HO heuristic varies as a function of the number of search agents for various system configurations. As the plots suggest, selecting 70 search agents provides the best compromise between solution optimality and computational tractability, with performance stabilizing while avoiding diminishing returns from additional agents.

A. Model and heuristic validation

To evaluate the accuracy of our stochastic geometry results (Section IV), and their sensitivity to the spatial assumptions, we performed an initial set of experiments under a static scenario in a region comprising a single area. Multiple configurations were considered, varying both the user and BS densities. The validation at the given configurations has been performed through Monte Carlo simulations.

Results are summarized in Table II. In all of the setups considered, the analytical values fall within the 95% confidence

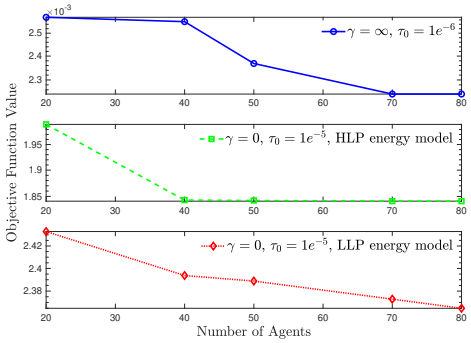


Figure 3. Performance of the HO algorithm for different numbers of agents and system configurations.

interval of the corresponding simulation outcomes. Note that, since the violation probability is dominated by the tail of the per-bit delay distribution and is therefore highly sensitive to both modeling approximations and finite-sample noise in simulation, in some configurations, the gap between the analytical and simulated values is relatively large. In any case, the violation probability observed in the simulations consistently remains below the target threshold of 5%. These findings indicate that, under the adopted spatial model (PPP-distributed static BSs and UEs, PCLP-distributed moving BSs), the proposed analytical approach accurately captures system behavior across the considered ranges of user and BS densities. To obtain a first indication of the sensitivity of our results to the Poisson assumption for the static BS layout, we have considered a scenario in which static BSs are distributed as a $\alpha-$Ginibre point process while moving BSs and UEs are still modeled as a PCLP and a PPP, respectively. An $\alpha-$Ginibre point process is a repulsive Determinantal Point Process (DPP) [57], [58] that models the fact that in actual deployments base stations are seldom very close to each other. The parameter α can be tuned to vary the amount of repulsion between BSs as a function of their distance. Such a repulsive model is expected to lead to a decrease in the mean distance between the user and its serving BS, to a decrease in its variance, and thus to (slightly) more efficient deployments, for a same mean BS density. Table II also shows how user-perceived performance changes when we choose repulsive point processes for static base station layouts. Given the more regular spacing of the macro BSs, the typical user is in general better served because the Ginibre process has a repulsion that prevents two BSs from being close together, and this reduces the heavy tail of the interference distribution. For small moving, the effect goes via interference: more regular macros mean less variance in macro interference at PCLP users.

To evaluate the effectiveness of our HO heuristic, we ran another set of experiments with the same configurations and compared the HO solutions for Problem 1 (Section V) with those obtained via exhaustive grid search across a large set of parameter combinations. In all tests and for all configurations, progressive grid refinement converged to solutions within at most 0.1% of those of our HO heuristic. This suggests that the HO heuristic can achieve a high level of effectiveness while reducing computation time by several orders of magnitude with respect to greedy approaches.

B. CAPEX-optimal configurations

1) Two-tier scenario: For a first characterization of the key performance patterns of the system, and in particular the impact of BS mobility on resource efficiency, in another set of experiments, we focused on a two-tier heterogeneous network scenario with IAB, consisting of macro BSs, and of moving small cell BSs. The scenario considered is a region partitioned into two equal-sized areas, modeling a simplified urban setup with a residential and an office/business area. Indeed, urban areas are known to exhibit complementary traffic patterns: office districts experience peak network demand and vehicle density during working hours, while residential areas remain low during daytime. These patterns reverse during late afternoon and evening commutes, creating a strong spatiotemporal correlation between vehicular presence and service requirements.

In such a scenario, we have assumed the two areas have symmetric patterns of user densification (i.e., when one area experiences a peak in user density, the other experiences a low, and vice versa) and that peaks and lows of user density are the same in both areas.

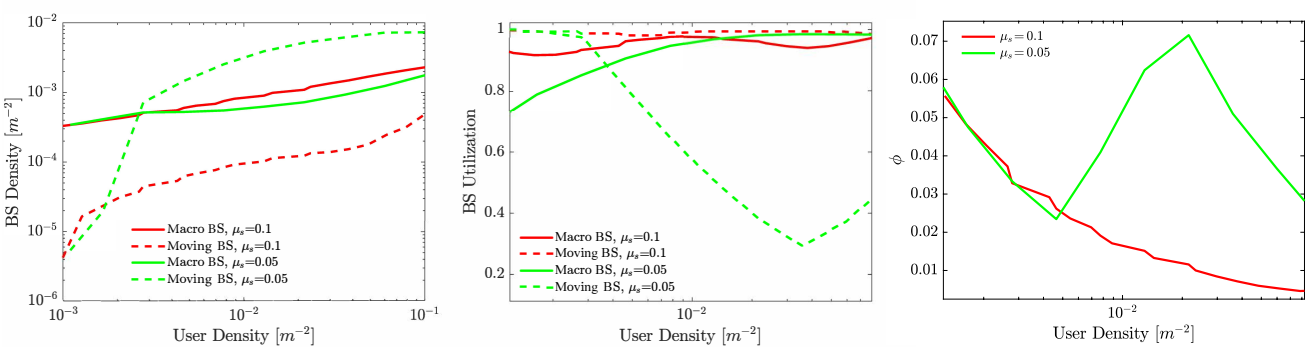
For a first assessment, we assumed no upper bounds on vehicular BS density, and we solved Problem 1 with the objective function accounting only for CAPEX costs (i.e., $\gamma \to \infty$). The goal has been to investigate the impact of unitary cost on the CAPEX-optimal system configuration, under different user densities and target QoS requirements. As the lows in user density do not affect the CAPEX optimization, we varied only the peak user density, assuming a low user density of 10^{-4} users per m^2, entirely served by macro BSs.

For the ratio μ_s between the unitary cost of macro cell BSs and that of small cell BSs, we considered values within the interval $(4, 25)$, as per experimental values [59]. The ratio is typically larger in city center settings, where macro site acquisition costs and construction costs typically dominate.

Fig. 4 summarizes results for different values of μ_s. The experiments show that, at low to medium user densities, in CAPEX-optimal configurations, users are mainly served by macro cell BSs, and moving small cell BSs are a small fraction of the total deployed. That is, in those settings, the resource efficiency enabled by moving BSs does not offset the wireless backhaul (BH) resource consumption and the communication inefficiency caused by a larger mean user-BS distance.

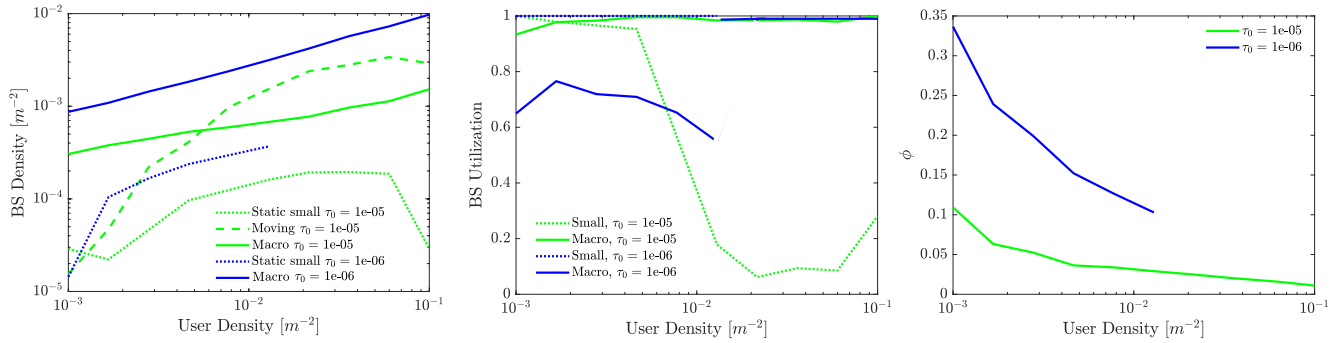
For higher user densities and sufficiently low relative unitary costs for moving BSs instead, the use of moving BSs becomes CAPEX-optimal, and users are mainly served by moving BSs. When this happens, the main role of macro BSs becomes that of access points for the wireless BH link of moving base stations, delegating the bulk of fronthaul service to moving BSs.

Fig. 4(b) shows the BS utilization at the optimum for macro and small cells. At a high relative cost, the BS utilization is very close to one, as this minimizes the number of BSs (static or moving) required to serve users with a given target QoS. Instead, when the relative cost of moving BSs is lower, and their density at the optimum is substantially larger than that of macro BSs, our optimization framework finds it more



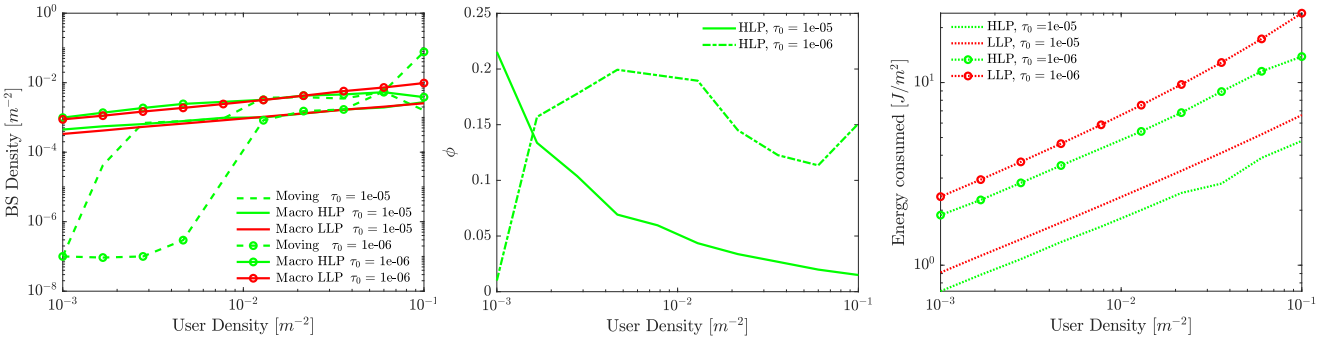
(a) (b) (c)

Figure 4. Two-tier scenario: CAPEX-optimal network configurations as a function of peak user density, for different relative BS unitary cost μ_s (ratio between the unitary cost of static macro and small cells), with $\tau_0 = 10^{-5}$. (a) Optimal BS densities; (b) Mean BS utilization at optimum; (c) WPS weight at optimum for users.



(a) (b) (c)

Figure 5. Three-tier scenario: CAPEX-optimal network configurations as a function of peak user density, for different target QoS values, for relative BS unitary costs $\mu_s = 0.05$ and $\mu_m = 0.01$ (ratio between the unitary cost of small and macro, and moving and macro, respectively). (a) Optimal BS densities; (b) WPS weight at optimum for users; (c) Mean BS utilization at optimum. Missing data points on the blue dashed curve in Fig. 5(a) and solid blue curve in Fig. 5(c) indicate parameter regions in which optimal solutions deploy no small cell base stations (i.e., neither static nor moving).



(a) (b) (c)

Figure 6. Two-tier scenario: (a) Energy-optimal BS densities vs peak user density, and (b) WPS weight for users at the optimum vs peak user density; (c) Network energy consumption over $24h$ per unit area at the optimum, for different configurations in terms of Macro BS energy models and target user-perceived QoS.

CAPEX-efficient to have a higher number of moving BSs with a lower utilization (green dashed curve in Fig. 4(b)), rather than to minimize their density and have them at utilization close to one. This is due to the impact on CAPEX (through the impact on macro BSs resources) of BH. That is, in this configuration, the cost of backhaul links dominates the overall cost of the moving BS paradigm. However, for large peak user densities, this trend inverts, and the utilization of moving BSs starts growing again with peak user density.

This pattern is evident also in Fig. 4(c), which shows the WPS weight of users at the macro BS at the optimum, as a function of user density. As expected, in the configuration with high relative cost for moving BSs, when increasing user density, macro BSs allocate an increasing amount of resources to BH links (and thus a lower amount to users), as they carry a larger amount of traffic. However, in the lower relative cost scenario (green curve in Fig. 4(c)), when the vast majority of users start being served by moving BSs, the WPS weight of users served at the macro BS increases. Indeed, at those user densities, users served by macro BS are few, and BH links do not carry a lot of traffic, as moving BSs are relatively dense and each serves very few users. However, when the user density is further increased, the trend inverts, as the resource cost of guaranteeing QoS for BH links becomes prevalent again.

2) Three-tier scenario: For a more realistic evaluation, and to better characterize the impact on CAPEX optimality of BS mobility, separating it from the cost of wireless BH, we extended our analysis to a three-tier (macro BSs, small static BSs, and moving BSs) scenario, in which both small static BSs and moving BSs employ in-band wireless backhauling. To account for the lower installation and deployment costs of moving BSs, we set $\mu_s = 0.05$ and $\mu_m = 0.01$.

As Fig. 5(a) shows, with a target per-bit delay of 10^{-5} s, the optimal configuration is very similar to that of the two-tier scenario. That is, for medium-to-high user densities, users are mainly served by small cells. In addition, except for scenarios with very low peak user densities (less than 2×10^{-3} users$/m^2$) moving small cell BS are clearly more CAPEX-efficient than static ones. In this configuration, as Fig. 5(b) suggests, and similarly to the two-tier scenario with $\mu_s = 0.05$, the higher the ratio between moving BSs and macro BSs (and thus, the higher the mean number of BH connections that a macro BS has to serve), the lower the moving BS utilization at optimum. This indeed allows lowering the resource requirements of BH links at the macro BS, making it easier to serve BH connections with the required QoS.

Instead, for a tighter target per-bit delay perceived by users, the experiments show that small cells (both static and moving) are not CAPEX efficient. This is due to the increase in the service capacity (and the related CAPEX cost) required by BH links at the macro BS.

Thus, in optimal configurations, access is implemented mainly via macro BSs, reducing to a minimum the use of small cell BSs (for low user densities) or not using them at all (for medium/high user densities). Note that, despite being way less dense than macro BS, small cell BS have a non-negligible impact on the system. As Fig 5(b) shows, when small cells are present, macro BS utilization is never more than 0.8, to cater for the (rare) wireless BH links and the statistical fluctuations in the resources they require. Note in this case that moving BSs are not present at all in the optimal solution. Indeed, under the adopted PCLP model, moving BSs cluster slightly more than PPP-distributed static small cells. As a result, the probability for a macro BS to serve the BH link of more than one moving BS is higher in moving BS than in static small cells, making the latter more CAPEX efficient than the former.

The experiments also show that for larger peak user densities, rising resource-requirements for BH links imply that small cells are altogether absent from the optimal solution. As expected, in these configurations, macro BS utilization at the optimum is very close to one.

Sensitivity to the macro BS layout. To assess the sensitivity of the static-to-moving transition to the macro BS layout, we replaced the PPP of macro BSs with an α-Ginibre process [58], leaving static small cells, moving BSs, and UEs unchanged, and re-solved the CAPEX optimization for $\tau_0 = 10^{-5}$ s. The distance between a user and its serving macro BS follows in closed form from the void probability of the process, while the cell-area distribution, which has no closed form, is fitted via Monte Carlo. Defining the transition point λ_u^{tr} as the user density at which the optimal densities of macro and moving BSs are equal, repulsion shifts it from $5.5 \cdot 10^{-3}$ users/m^2 (PPP) to $2.9 \cdot 10^{-2}$ ($\alpha = 0.5$) and $5.2 \cdot 10^{-2}$ users/m^2 ($\alpha = 1$). The macro (and moving) BS density at λ_u^{tr} is of the same order of magnitude in the three cases ($5.5 \cdot 10^{-4}$, $8.9 \cdot 10^{-4}$, and $7.6 \cdot 10^{-4}$ m^{-2}). A more regular macro layout removes the poorly covered regions and large, overloaded cells typical of the PPP, so each macro BS serves more users within the target QoS, and macro BSs remain the dominant tier even at higher user densities. Hence, while the qualitative pattern of the transition is preserved, the transition point is sensitive to the macro BS layout.

C. Energy-optimal configurations

As already observed, another potential advantage of cellular networks with moving BSs is a higher energy efficiency of network operations. Indeed, by tracking spatiotemporal peaks in service demand, moving BSs enable spatial resource reuse, avoiding the baseline energy consumption of static BSs that remain powered (or in low-power sleep states) during low-traffic periods. Thus, in a new set of experiments, we solved Problem 1 while accounting only for network OPEX, and specifically, only for energy costs. The scenario considered is again the two areas, three-tier setup of the previous section. As for the BS energy model, we have considered two setups. In the first one, reflecting many present-day network configurations, the macro BS energy model is LLP, while in the second one, it is HLP. In both setups, small cells have an HLP energy model.

The energy-optimal configurations are summarized in Fig. 6, in which the x-axis shows the peak user density. These plots indicate that, independently from the target QoS for users, when macro BSs are LLP, the energy cost of BH links (and thus of moving BSs) is high. Thus, in these configurations (red curves in Fig. 6(a)), no moving BS is deployed, and users are served only by macro BSs. Instead, when the energy model for macro BSs is HLP, at medium-to-high peak user densities, it becomes more energy-efficient to serve users with moving BSs. Moreover, the tighter the target mean user throughput, the higher the minimum peak user density at which deploying moving BSs is more energy efficient than static deployments. This is because, as can be verified from the expressions in Theorem 3, keeping all else constant, tighter target per-bit delays lead to an increase in violation probability, making BH links (and therefore, moving BSs) more resource-intensive for the same amount of traffic served.

Interestingly, particularly for a target per-bit delay of 10^{-5}, the OPEX-optimal configurations in terms of static and moving BS density and WPS weight per user (Fig. 6(b)) are very similar to CAPEX-optimal configurations. However, as far as the WPS weights for users are concerned, we observe that, for a target per-bit delay of 10^{-6}, when moving BS density at the optimum is low, the optimal WPS weight tends to increase when increasing peak user density, instead of decreasing, for low-to-medium peak user densities. This behavior is the norm when macro BSs serve mainly users, and moving BSs are rare. Indeed, in those cases, when density increases, every user requires more resources (and thus more BS time) to be served, due mainly to interference. However, when moving BSs start to be prevalent in the scenario, BH links require a substantial

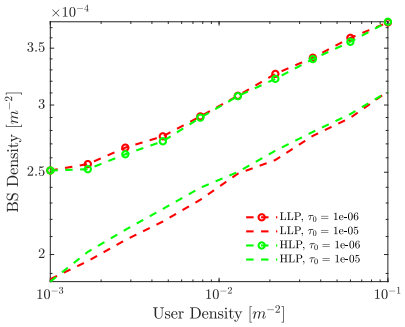


Figure 7. TCO-optimal density of moving BSs as a function of peak user density, for different energy models in the LEO backhauling scenario.

amount of macro BS time, and the WPS weight for users stops increasing. Only at very high peak user densities, when interference levels are high, the WPS weight of users starts increasing again.

Finally, Fig. 6(c) shows the energy consumed at the optimum over 24 h as a function of the peak user density. These plots show that the optimization consistently leads to a sublinearity of the energy consumed by the network as a function of peak user density, despite the resource cost of BH links.

D. LEO Backhauling scenario

To further investigate the impact of BH links on resource efficiency in networks with moving BSs, we have analyzed the TCO-optimal network configuration in the two-area, three-tiers scenario of Section VI-B, assuming that wireless BH for both static small cell BSs and moving BSs is implemented via LEO satellite links rather than in-band. Unless otherwise stated, parameter μ in the objective function in Problem 2 has been set to one, thus assuming no difference in unitary cost of energy between different BS classes, and $\gamma = 1$. In addition, μ_m and μ_s have also been set to one. That is, we consider the case in which backhauling via LEO satellites makes the CAPEX cost of small BSs (both static and moving) comparable to that of macro BSs. Despite such a conservative assumption, across all of the settings considered (all peak user densities, and all target per-bit delay values), satellite backhauling leads to optimal configurations where the density of macro BSs and static small cell BSs at the optimum is zero, and users are served exclusively by moving BSs. This occurs because out-of-band LEO backhauling dedicates separate spectral resources for backhaul traffic, unlike the IAB scenario, where access and backhaul share spectrum. This allows moving BSs to operate without backhaul capacity constraints and without the interference it brings, resulting in substantially more resource-efficient operation than in the IAB case.

As shown in Fig. 7, the relationship between the optimal moving BS density and the peak user density is again well approximated by a power law. As expected, increasing the required throughput results in a higher overall density of deployed moving BSs (and thus a higher TCO), but the optimal configuration is always implemented only with moving BSs. Even when increasing the CAPEX cost of moving BSs to account for the HW and installation costs of LEO backhauling (by setting $\mu_m = 1.5$ [3] in Problem 2), the optimal configuration remains one in which only moving BSs are deployed.

To account for satellite subscription costs and the energy overhead of satellite communications, we performed a sensitivity analysis by varying the parameter μ in Problem 2 over the range $[1, 5]$, where μ scales the additional operational cost of LEO backhauling relative to terrestrial infrastructure. Across all tested cost multipliers, the TCO-optimal configurations exclusively deployed moving BSs, showing that this outcome is insensitive to satellite service pricing within the tested range. Bottom line, these results suggest that dedicated backhauling unlocks full reliance on moving BSs across all regimes, isolating BH costs, including spectrum sharing and macro utilization, as the primary efficiency bottleneck in networks with moving BSs.

E. Practical deployment considerations

The practical feasibility of the moving network paradigm depends on several deployment constraints and open issues that lie beyond the scope of the analytical framework presented here. We discuss the most relevant ones below.

Selection of BS-equipped vehicles: The formulation of Problems 1 and 2 in Section V assumes that the vehicles equipped with a BS are selected uniformly at random within each area and time slot. In practice, more sophisticated strategies that prioritize sub-fleets with favorable and predictable mobility patterns (e.g., public transport or ride-sharing vehicles along recurrent commuting corridors) are expected to better match moving BS availability with traffic peaks. Such strategies may further improve resource utilization and reduce the CAPEX of moving BS deployments with respect to the predictions of our framework.

Spatial clustering: Our numerical results are derived under PPP/PCLP spatial assumptions, and our sensitivity analysis (Sections VI-A and VI-B) only covers repulsive (α-Ginibre) static BS layouts. Real deployments may exhibit clustering at scales smaller than the considered areas, e.g., UE concentrations around transport hubs or venues, static small cells deployed specifically at hotspots, and vehicles bunched in congested corridors or parking lots. The effect of such clustering on the optimal infrastructure mix cannot be determined a priori. On the one hand, UE clustering increases the variance of the per-cell load, and hence the tail of the BH traffic demand, which would penalize in-band backhauled small cells. On the other hand, a positive spatial correlation between vehicle and UE clusters, which is precisely what motivates the natural MN paradigm, may favor moving BSs. Quantifying these effects requires extending the framework to clustered and correlated point processes, which we leave for future work.

Participation incentives: Natural moving networks rely on vehicular users acting as "prosumers", who temporarily contribute their vehicles to the RAN as mobile infrastructure. Realistic deployments will therefore require incentive and compensation mechanisms (e.g., revenue sharing, subscription discounts, or third-party contracts with fleet operators). While

[3]Note that further increasing this value would not be realistic, as, in general, the cost of small cells is lower than that of macro cells.

their costs can be incorporated into the CAPEX/OPEX terms of Problems 1 and 2, their design and adoption dynamics remain an open research problem.

Interference management: The high mobility of vehicle-mounted BSs, together with their tight spectral coupling with macro cells (also due to IAB), complicates frequency planning and increases the likelihood of co-channel interference compared with fully static RANs. Effective large-scale deployments therefore require robust, dynamic interference management and mobility-aware coordination schemes (e.g., adaptive power control, interference-aware scheduling, or predictive beam and handover management) to preserve network stability and meet the target QoS guarantees.

VII. Conclusions

In this work, we address a critical gap in vehicular-enhanced Beyond-5G/6G network design by proposing a stochastic geometry framework for quantifying the resource efficiency achievable through the deployment of moving BSs under realistic wireless backhauling constraints. Our QoS-aware optimization minimizes CAPEX/OPEX while accounting for interference, road-grid mobility, and complex access-backhaul interactions. We have characterized how the optimal infrastructure mix and TCO vary with user density, traffic load, and cost ratios. A sensitivity analysis with respect to the macro BS layout, modeled as a repulsive α-Ginibre process, shows that the qualitative structure of the optimal configuration is preserved, while the static-to-moving transition moves to user densities up to one order of magnitude higher. This indicates that PPP-based thresholds are optimistic for moving BSs, and that the transition point should be evaluated for the specific macro layout at hand. Under the adopted PPP/PCLP spatial models and idealized assumptions (path-loss-only channel, downlink traffic, uniformly selected BS-equipped vehicles), numerical results suggest that moving base stations enable substantial resource efficiency gains in medium-high user density scenarios, where they effectively serve fronthaul traffic despite the inherent resource constraints and impairments of in-band integrated access and backhaul architecture.With an ideal out-of-band LEO backhaul, instead, TCO-optimal configurations rely exclusively on moving BSs, suggesting that in-band backhauling is one of the key factors limiting the efficiency of moving networks. These findings indicate that integrating the moving network paradigm with energy-proportional base station models holds the potential to reduce the need for dense static infrastructure deployments and to increase network energy efficiency. Future research may extend the analysis to clustered and spatially correlated distributions of UEs and BSs, and to non-terrestrial integrations and steerable vehicles, such as UAV or 3D mobility scenarios, to capture the broader scope of 6G architectures, and to account for the effects of handover on user-perceived performance.

Appendix

A. Proof of Lemma 1

The formula is derived by computing the Palm expectation of the total received interfering power $I(D) = \sum_{i\in\Phi_M^z} P_M r_i^{-\alpha} u_i + \sum_{i\in\Phi_S^z} P_S r_i^{-\alpha} u_i$ for a user distant D from the serving BS, where $u_i = 1$ if the BS is active, Φ_M^z is the PPP of static macro cells in area z, and Φ_S^z is the point process of small cells given by the superposition of the point processes of small static and moving cells. The final formula is derived from considering that BSs are active only for a fraction of time equal to their utilization and that both static and moving BSs contribute to inter-BS interference.

B. Proof of Theorem 1

Lemma 3. *The cumulative distribution function of the distance between the typical user at the origin and the closest point of the PLCP Ξ, in area z, is*

$$CDF_{PLCP}(r) = 1 - e^{-2\pi\lambda_l \int_0^r (1-\exp(-2\lambda_m^z \sqrt{r^2-u^2})du} \quad (14)$$

Proof. We begin by calculating the complement of the void probability [60], which is the probability that there are no points of Ξ inside the ball of radius r centered at the origin, denoted by $B(0,r)$. Let $N_p(B(0,r))$ represent the number of points of Ξ in $B(0,r)$; then, the void probability is given by:

$$\begin{aligned}
&P\big(N_p(B(0,r)) = 0\big) = P\Big(N_p\Big(\bigcup_{l_i\in\Phi_l} (l_i \cap B(0,r))\Big) = 0\Big) \\
&= \mathbb{E}_{\Phi_l}\Big[\prod_{l_i\in\Phi_l} P\big(N_p(l_i \cap B(0,r)) = 0 \,\big|\, \Phi_l\big)\Big] \\
&= \mathbb{E}_{\Phi_l}\Big[\prod_{l_i\in\Phi_l} \exp\big(-\lambda_m^z\, \nu(l_i \cap B(0,r))\big)\Big] \\
&= \exp\Big(-\lambda_l \int_0^{\pi}\int_{-r}^{r} \big(1 - e^{-\lambda_m^z \nu(l(u,\theta)\cap B(0,r))}\big)\, du\, d\theta\Big) \\
&= \exp\Big(-2\pi\lambda_l \int_0^r \big(1 - e^{-2\lambda_m^z\sqrt{r^2-u^2}}\big)\, du\Big)
\end{aligned}$$

In this derivation, we used the fact that on each line l_i the void probability corresponds to that of an independent 1D PPP with intensity λ_m^z. Here, ν denotes the Lebesgue measure on $\mathbb{R}$, and the last equality follows from applying the probability generating functional of the 2D PPP defined on the cylinder $C = [0,\pi)\times\mathbb{R}$ with intensity $\Lambda(drd\theta) = \lambda_l\, drd\theta$ [28]. □

Since the transmit power of each of the populations is different, if the distance from a BS of population 1 with transmission power P_M is r, the distance from a BS of population 2 transmitting at P_S such that the received power will be the same as for the BS from population 1 is $r' = r\rho = r\sqrt[\alpha]{\frac{P_S}{P_M}}$

Let R_1, R_2, and R_3 denote the distance between the typical user and the closest SMC, SSC, and MSC, respectively. As R_1, R_2, and R_3 are independent random variables, letting $R = min(R_1, R_2, R_3)$ we have that the CDF of R is $CDF_R(r) = 1 - \prod_{n=1}^{3}(1 - CDF_{R_n}(r))$ The CDF of R_1 and R_2 can be easily obtained from the void probability of a PPP computed in $B(0,r)$ and $B(0,\rho r)$ respectively. The CDF of R_3 is obtained in a similar way, where the void probability of the PLCP is computed as in Lemma 3. Thus, we have:

$$CDF_R(r) = 1 - e^{-\pi r^2(\lambda_M^z + \lambda_s^z\rho^2) - 2\pi\lambda_l \int_0^{\rho r}(1-e^{-2\lambda_m^z\sqrt{(\rho r)^2-u^2}})du}$$

The PDF is obtained by deriving with respect to r the equation for the CDF of R.

C. Proof of Theorem 2

We will focus on the derivation of $\bar{\tau}_M^z$ while the derivation of the first formula follows the same line as in [31]. The computation of the Palm expectation of Eq. 2 follows a similar approach to that in [45]:

$$\bar{\tau}_M^z = E^0\left[\frac{N_s(S(0)) + N_m(S(0)) + \phi^z N_U(S(0))}{\phi^z C(D(0), P, I)}\right] = \int_0^\infty \frac{E^0[N_s + N_m + \phi^z N_U \mid r \le D \le r + dr]}{\phi^z C(D, P, \bar{I})} \cdot P(r \le D \le r + dr)$$

where $\bar{I}$ is given by Lemma 1. For $dr \to 0$ we have $P(r \le D \le r + dr) \approx f_R^z(r)$ with $f_R^z(r)$ as in Eq. 4. $E^0[N_s + N_m + \phi^z N_U | r \le D \le r + dr]$ is the Palm expectation of the random variable describing the number of users served by the same BS serving the typical user at distance D. It can be rewritten as $E^0[N_s + N_m | r \le D \le r + dr] + E^0[\phi^z N_U | r \le D \le r + dr]$. Leveraging Cambpell's theorem in polar coordinates with $f(x, \theta) = \mathbf{1}_{(S(x,\theta)=S | r \le D \le r+dr)}$, we can rewrite the second expectation as:

$$E^0\left[\int_0^\infty \int_0^{2\pi} \mathbf{1}_{(S(x,\theta)=S|r\le D\le r+dr)} \phi^z \lambda_u^z d\theta x dx\right] = = \int_0^\infty \int_0^{2\pi} \phi^z \lambda_u^z P(S(x,\theta) = S | r \le D \le r + dr) d\theta x dx$$

To derive the probability inside the integral we proceed as in [49] and we move the typical user in $(0, -r)$ so that its serving static BS is located at the origin. Then we consider a user in (x, θ) served by the macro BS at the origin and impose that no other BSs (of any tiers) are closer. If $A(r, x, \theta)$ is the area of the circle centered at (x, θ) that is not overlapped by the circle centered at the typical user, we should impose that no macro BS are in that area and no small BS are in $A(r, \rho x, \theta)$. The scaling factor ρ accounts for the difference in transmission power. Using the independence of the BS tiers PP, and their void probabilities, the event of not having other BS serving the user in (x, θ) has probability:

$$e^{-\lambda_M^z A(r,x,\theta) - \lambda_s^z A(r,\rho x,\theta) - 2\pi\lambda_l \int_0^{r_A} (1 - \exp(-2\lambda_m^z \sqrt{r_A(\rho)^2 - u^2}) du}$$

where $r_A(z) = \sqrt{\frac{A(r,zx,\theta)}{\pi}}$ is the radius corresponding to the same area. For the PLCP process, the area is computed as the one generated by a BS of a PPP with a mean intensity equal to the mean intensity of the PLCP.

When the serving base station is small, the computation is slightly different because x corresponds to the radius of the circle where no other small cell should be located. To ensure that no other macro BS is serving the user in (x, θ), we should consider the circle with radius x/ρ Similarly, we compute $E^0[N_s + N_m | r \le D \le r + dr]$, but this time we only account for static macro cells serving as the base station for the BH. Thus, the Voronoi cell area has expression $h_{BH}^z(r) = \int_0^\infty \int_0^{2\pi} e^{-\lambda_M^z A(r,x,\theta)} x d\theta dx$. The existence and uniqueness of the fixed point are established by applying the Banach fixed-point theorem to the fixed point problem at hand, defined on $(\mathbb{R}, \|\cdot\|_\infty)$. It can be demonstrated that the system of equations governing the average per-bit delays forms a contraction. This conclusion arises from the fact that both the average interference $\bar{I}$ and the capacity C are Lipschitz continuous in relation to $\bar{\tau}$ and $\bar{I}$, respectively.

We observe that the proof of convergence of the fixed point problem does not rely on any assumption on user density or traffic intensity. The fixed point problem is due to the fact that the expected ideal per-bit delay is a function of the mean BS utilization, which in turn depends on the ideal per-bit delay. When traffic intensity (user density) grows, BS utilization grows too, until it reaches its maximum value, equal to one. Thus, at that point, BS utilization is no longer a function of per-bit delay, and the fixed-point problem reduces to a closed-form expression for the ideal per-bit delay. Thus, the fixed-point problem has a valid solution in any condition of traffic intensity or user density.

D. Proof of Lemma 2

For simplicity, we drop the location indication, and we denote $S(0)$ and $D(0)$ as S and D respectively. $CDF_r(r)$ is the cumulative distribution function of the distance of users from their serving static macro base station derived from the probability of not having other SBS than the serving one in the annulus of radius r and $r + dr$. To prove the result, we need to compute the mean per bit-delay in downlink for moving and static small cells as a measurable function $g(r)$. In Euclidean space with Lebesgue measure, measurable functions are continuous. The per-bit delay perceived by a SC (static or moving) in BH as $\tau_{BH} = (N_s + N_m + \phi N_U)/C(D, P_M, I)$ To obtain $g(r)$, we compute the number of users and small cells served by the static BS in S as a function of r. For the PPP with density $\lambda_m + \lambda_s + \phi\lambda_u$, this quantity has expression $(N_s + N_m + \phi N_U)(r)$. Using Campbell's theorem, its mean value is thus given by $(\lambda_s + \lambda_m) h_{BH}(r) + \phi_u \lambda_u h_M(r)$, where $h_M(r)$ and $h_{BH}(r)$ are the mean areas of the Poisson Voronoi cell of a static macro BS, respectively with and without accounting for other BS tiers in the system, conditioned to having the user or the small cells at a distance r from its serving BS. Their derivation follows as in the proof of Theorem 2.

E. Proof of Theorem 3

We consider a small BS cell in the region z serving N_U BB users.

Proposition 1. *For $\lambda_u^z < 1$, the variance of the PPP of users is lower than the variance of the Poisson Voronoi cell area.*

Proof. The variance associated with the number of users in a generic Voronoi cell of area A is equal to the density $\lambda_u^z A$. Also, if the user density is lower than 1, then the average size of Poisson Voronoi cells associated with BS is $\ge 1\ m^2$. The variance of the surface of Poisson Voronoi cell A can be derived from the second moment as $Var(A) = \frac{2}{7}\left(\frac{1}{\lambda_M^z + \rho\lambda_m^z\lambda_l\pi + \rho\lambda_s^z}\right)^2$. Since the ratio between the density of users and BS is always greater than 1, then $(\lambda_M^z + \rho\lambda_m^z\lambda_l + \rho\lambda_s^z) < 1$, and the result follows. □

Due to this assumption, the stochasticity of the per-bit delay is only associated with the cell area rather than being influenced by fluctuations in the number of users.

Lemma 4. *When the utilization of the small cell is less than 1, the PDF of the per-bit delay of the backhauling traffic*

demand in downlink for a small cell in area z is $f_{\tau_d}(t) = a^{\frac{7}{2}} \frac{343}{15} \sqrt{\frac{7}{2\pi}} t^{-\frac{9}{2}} e^{-\frac{7}{2}\frac{a}{t}}$, *with* $a = \frac{\tau_0}{\lambda_u^z}(\lambda_M^z + \rho\lambda_m^z\lambda_l + \rho\lambda_s^z)$.

Proof. We consider the worst case in which users always have data to download. When the utilization of the small cell is less than 1, for the assumption made on the BS service model, the small cell is serving each user with a mean per-bit delay corresponding to the target value, equal to τ_0. Thus the mean per bit delay of the aggregate traffic demand is $\tau_d = \frac{\tau_0}{N_U}$. For Proposition 1, the PDF of τ_d is dominated by the stochasticity of the area of the cell of the small cell. Thus the random variable τ_d can be written as $\tau_d = \frac{\tau_0}{\lambda_u^z A}$ where A is the area of the Voronoi cell of the small cells. An exact analytical expression of the probability distribution of the area of a Poisson Voronoi tessellation is available only in the single-dimension case. However, accurate approximations are available for the two-dimensional case. The PDF $f_A(y)$ of the normalized area of a Voronoi cells is $f_A(y) = \frac{343}{15}\sqrt{\frac{7}{2\pi}} y^{\frac{5}{2}} e^{-\frac{7}{2}y}$, where y is the area of the Poisson Voronoi cell divided by the average surface given by $1/(\lambda_M^z + \rho\lambda_m^z\lambda_l\pi + \rho\lambda_s^z)$ where $\rho = \sqrt[\alpha]{P_S/P_M}$ accounts for the different transmission powers of the network tiers. The expression for the PDF f_{τ_d} of the per-bit delay associated with the aggregate traffic demand in downlink is derived from $f_{\tau_d}(\tau) = f_A(g^{-1}(\tau))\left|\frac{d}{d\tau} g^{-1}(\tau)\right|$, with $\tau_d = g(A) = \frac{\tau_0}{\lambda_u^z A}(\lambda_M^z + \rho\lambda_m^z\lambda_l\pi + \rho\lambda_s^z)$. □

We now derive the violation probability, i.e. the probability that the per-bit delay perceived by the backhauling connection is insufficient to carry the aggregate traffic demand (that is, that it is larger than τ_d). Given that with τ_{BH}^z we denote the ideal per-bit delay perceived by the backhauling connections, the actual per-bit delay of the backhauling connections is given by $\tau_{BH}^z/\bar{U}_M^z$, where $\bar{U}_M^z$ is the mean utilization of static macro cells in z. We thus have that the violation probability can be expressed as $V^z = P\left(\frac{\tau_{BH}^z}{\bar{U}_M^z} > \tau_d\right) = P\left(\tau_{BH}^z > \bar{U}_M^z\,\tau_d\right)$. Since τ_d and τ_{BH}^z are independent, conditioning on τ_d and applying the law of total probability gives $\int_0^\infty f_{\tau_d}(x)\,P\left(\tau_{BH}^z > \bar{U}_M^z\,x\right)dx$ $= \int_0^\infty f_{\tau_d}(x)\left(1 - CDF_{\tau_{BH}^z}\left(\bar{U}_M^z\,x\right)\right)dx$, where $f_{\tau_d}(\cdot)$ is the pdf derived above and $CDF_{\tau_{BH}^z}(\cdot)$ is the CDF of the ideal per-bit delay of the backhauling connections.

ACKNOWLEDGMENT

The authors used ChatGPT (GPT-5) only for rephrasing and improving the clarity of author-generated text.

REFERENCES

[1] C.-X. Wang and al., "On the Road to 6G: Visions, Requirements, Key Technologies, and Testbeds," *IEEE Commun. Surveys Tuts.*, vol. 25, no. 2, pp. 905–974, 2023.

[2] W. Hurst, S. Evmorfos, A. Petropulu, and Y. Mostofi, "Uncrewed Vehicles in 6G Networks: A Unifying Treatment of Problems, Formulations, and Tools," *Proc. IEEE*, vol. 113, no. 9, pp. 952–986, 2025.

[3] I. Akyildiz and H. Guo, "Holographic-type communication: A new challenge for the next decade," *ITU J. Future Evol. Technol.*, vol. 3, pp. 421–442, 09 2022.

[4] X. S. Shen, J. Gao, M. Li, C. Zhou, S. Hu, M. He, and W. Zhuang, "Toward Immersive Communications in 6G," *Front. Comput. Sci.*, vol. 4, p. 1068478, 2023.

[5] 6G-IA, "6G IA Position Paper: FP10 and Beyond SNS," 6G Smart Networks and Services Industry Association, Tech. Rep., May 2025. [Online]. Available: https://6g-ia.eu/wp-content/uploads/2025/05/sns-in-fp10-position-papervfinal.pdf

[6] GSMA, "Vision 2040: Spectrum for the Future of Mobile Connectivity," GSMA, Tech. Rep., Nov. 2025. [Online]. Available: https://www.gsma.com/connectivity-for-good/spectrum/wp-content/uploads/2025/11/Vision-2040-Future-Spectrum-Needs-v2.pdf

[7] H. Cho, S. Mukherjee, D. Kim, T. Noh, and J. Lee, "Facing to wireless network densification in 6G: Challenges and opportunities," *ICT Express*, vol. 9, no. 3, pp. 517–524, 2023.

[8] I. Trigui, S. Affes, M. D. Renzo, and D. N. K. Jayakody, "Coverage Analysis and Scaling Laws in Ultra-Dense Networks," *IEEE Trans. Commun.*, vol. 69, no. 6, pp. 4158–4171, 2021.

[9] J. Kibilda and G. de Veciana, "Dynamic Network Densification: Overcoming Spatio-Temporal Variability in Wireless Traffic," in *Proc. IEEE GLOBECOM*, 2018, pp. 1–6.

[10] M. S. Akbar, Z. Hussain, M. Ikram, Q. Z. Sheng, and S. C. Mukhopadhyay, "On challenges of sixth-generation (6G) wireless networks: A comprehensive survey of requirements, applications, and security issues," *Journal of Network and Computer Applications*, vol. 233, no. 104040, p. 104040, 2025.

[11] Samsung Research, "Energy Saving for 6G Network: Part I," *Samsung Research Blog*, 2025. [Online]. Available: https://research.samsung.com/blog/Energy-Saving-for-6G-Network-Part-I

[12] S. Jaffry, R. Hussain, X. Gui, and S. F. Hasan, "A Comprehensive Survey on Moving Networks," *IEEE Commun. Surveys Tuts.*, vol. 23, no. 1, pp. 110–136, 2021.

[13] Y. Liao, "Optimal Deployment and Operation of Robotic Aerial 6G Small Cells," *IEEE Commun. Mag.*, vol. 60, no. 9, pp. 80–86, 2022.

[14] F. Dressler, F. Klingler, and G. A. Rizzo, "Dynamic Mobile Base Stations in 5G Networks – The Moving Network Paradigm," in *The 5G Italy Book 2019: a Multiperspective View of 5G*. CNIT, 2019, pp. 477–492. [Online]. Available: https://www.ccs-labs.org/bib/dressler2019dynamic/dressler2019dynamic.pdf

[15] B. Kirubakaran, O. Vikhrova, S. Andreev, and J. Hosek, "UAV-BS Integration with Urban Infrastructure: An Energy Efficiency Perspective," *IEEE Commun. Mag.*, vol. 63, no. 3, pp. 100–106, 2025.

[16] M. Mozaffari, W. Saad, M. Bennis, and M. Debbah, "Wireless communication using unmanned aerial vehicles (UAVs): Optimal transport theory for hover time optimization," *IEEE Trans. Wireless Commun.*, vol. 16, no. 12, pp. 8052–8066, 2017.

[17] C. Li, A. Wang, G. Sun, and L. Liu, "Air Auxiliary Base Station Deployment Optimization in UAV-assisted IoT," in *Proc. IEEE WCNC*, 2022, pp. 872–877.

[18] T. Derrmann, R. Frank, F. Viti, and T. Engel, "How Road and Mobile Networks Correlate: Estimating Urban Traffic Using Handovers," *IEEE Trans. Intell. Transp. Syst.*, vol. 20, no. 8, pp. 3017–3032, 2019.

[19] F. Mohammadnia, M. Fiore, and M. Ajmone Marsan, "Adaptive Densification of Mobile Networks: Exploring Correlations in Vehicular and Telecom Traffic," in *Proc. Med-Hoc-Net*, 2018, pp. 1–8.

[20] M. Ajmone Marsan, F. Mohammadnia, C. Vitale, M. Fiore, and V. Mancuso, "Towards mobile radio access infrastructures for mobile users," *Ad Hoc Netw.*, vol. 89, pp. 204–217, 2019.

[21] Y. Nakayama, K. Maruta, T. Tsutsumi, and K. Sezaki, "Optically Backhauled Moving Network for Local Trains," in *Proc. ACM HotWireless*, 2017, pp. 31–35.

[22] S. Jangsher and V. O. Li, "Backhaul Resource Allocation for Existing and Newly Arrived Moving Small Cells," *IEEE Trans. Veh. Technol.*, vol. 66, no. 4, pp. 3211–3219, 2017.

[23] S. Zafar, S. Jangsher, M. Aloqaily, O. Bouachir, and J. Ben Othman, "Resource Allocation in Moving Small Cell Network using Deep Learning based Interference Determination," in *Proc. IEEE PIMRC*, 2019.

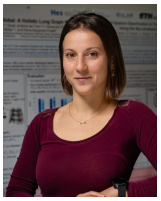
[24] A. Gupta, A. Heidari, J. Jin, and D. Bharadia, "Densify & Conquer: Densified, smaller base-stations can conquer the increasing carbon footprint problem in nextG wireless," *ArXiv*, vol. abs/2403.13611, 2024.

[25] C. Saha and H. S. Dhillon, "Millimeter Wave Integrated Access and Backhaul in 5G: Performance Analysis and Design Insights," *IEEE J. Sel. Areas Commun.*, vol. 37, no. 12, pp. 2669–2684, 2019.

[26] C. Madapatha, B. Makki, C. Fang, O. Teyeb, E. Dahlman, M.-S. Alouini, and T. Svensson, "On integrated access and backhaul networks: Current status and potentials," *IEEE Open J. Commun. Soc.*, vol. 1, pp. 1374–1389, 2020.

[27] C. Li, Q. Luo, G. Mao, M. Sheng, and J. Li, "Vehicle-Mounted Base Station for Connected and Autonomous Vehicles: Opportunities and Challenges," *IEEE Wireless Commun.*, vol. 26, no. 4, pp. 30–36, 2019.

[28] C.-S. Choi and F. Baccelli, "An Analytical Framework for Coverage in Cellular Networks Leveraging Vehicles," *IEEE Trans. Commun.*, vol. 66, no. 10, pp. 4950–4964, 2018.
[29] C. T. Cicek, H. Gultekin, B. Tavli, and H. Yanikomeroglu, "UAV Base Station Location Optimization for Next Generation Wireless Networks: Overview and Future Research Directions," in *Proc. Int. Conf. Unmanned Veh. Syst.-Oman (UVS)*, 2019, pp. 1–6.
[30] V. Mandawaria, C. Majumdar, A. Chaudhari, N. Sharma, A. Nigam, B. Jung, and J. Jung, "Performance Evaluation of B5G Moving Networks with Spatial Consistency and Random Blockages," in *Proc. IEEE WCNC*, 2021, pp. 1–6.
[31] L. Finarelli, F. Dressler, M. Ajmone Marsan, and G. Rizzo, "Assessing the Benefits of Ground Vehicles as Moving Urban Base Stations," in *Proc. MedComNet*, 2025, pp. 1–6.
[32] C.-S. Choi and F. Baccelli, "Poisson Cox Point Processes for Vehicular Networks," *IEEE Trans. Veh. Technol.*, vol. 67, no. 10, pp. 10 160–10 165, 2018.
[33] C.-S. Choi, J. Kim, and F. Baccelli, "Analysis of a Spatially Correlated Vehicular Network Assisted by Cox-distributed Vehicle Relays," *IEEE Trans. Veh. Technol.*, pp. 1–14, 2025.
[34] C.-S. Choi and F. Baccelli, "Extending the LOS Coverage of Vehicular Networks Based on Roadside Units and Vehicle Relays," in *Proc. IEEE ICC*, 2023, pp. 3977–3982.
[35] X. Li, Q. Wang, J. Liu, and W. Zhang, "3D Deployment with Machine Learning and System Performance Analysis of UAV-Enabled Networks," in *Proc. IEEE/CIC ICCC*, 2020, pp. 554–559.
[36] F. Liang, J. Zhang, B. Li, Z. Yang, and Y. Wu, "The Optimal Placement for Caching UAV-assisted Mobile Relay Communication," in *Proc. IEEE ICCT*, 2019, pp. 540–544.
[37] J. Zhang and T. Ratnarajah, "Performance Analysis of In-Band-Full-Duplex Multi-Cell Wideband IAB Networks," *IEEE Access*, vol. 12, pp. 47 024–47 040, 2024.
[38] M. Tayyab, X. Gelabert, and R. Jäntti, "A Survey on Handover Management: From LTE to NR," *IEEE Access*, vol. 7, pp. 118 907–118 930, 2019.
[39] A. Alkhateeb, I. Beltagy, and S. Alex, "Machine Learning for Reliable mmWave Systems: Blockage Prediction and Proactive Handoff," in *Proc. IEEE GlobalSIP*, 2018, pp. 1055–1059.
[40] Y. Ullah, M. B. Roslee, S. M. Mitani, S. A. Khan, and M. H. Jusoh, "A Survey on Handover and Mobility Management in 5G HetNets: Current State, Challenges, and Future Directions," *Sensors*, vol. 23, no. 11, p. 5081, 2023.
[41] B. Tezergil and E. Onur, "Wireless Backhaul in 5G and Beyond: Issues, Challenges and Opportunities," *IEEE Commun. Surveys Tuts.*, vol. 24, no. 4, pp. 2579–2632, 2022.
[42] Z. Abdullah, S. Kisseleff, E. Lagunas, V. N. Ha, F. Zeppenfeldt, and S. Chatzinotas, "Integrated Access and Backhaul via Satellites," in *Proc. IEEE PIMRC*, 2023, pp. 1–6.
[43] R. Favraud, A. Apostolaras, N. Nikaein, and T. Korakis, "Toward moving public safety networks," *IEEE Commun. Mag.*, vol. 54, no. 4, pp. 14–20, 2016.
[44] J. G. Andrews, F. Baccelli, and R. K. Ganti, "A Tractable Approach to Coverage and Rate in Cellular Networks," *IEEE Trans. Commun.*, vol. 59, no. 11, pp. 3122–3134, 2011.
[45] G. Rizzo, B. Boi, C. Esposito, and M. Ajmone Marsan, "A Stochastic Geometry Approach to Performance Modeling of SWIPT Vehicular Networks," in *Proc. WiOpt*, 2024, pp. 76–83.
[46] C. G. Tsiligkaridis, H. S. Dhillon, and J. G. Andrews, "Coverage Analysis of Relay-Assisted Cellular Networks with In-Band Backhauling," *IEEE Trans. Wireless Commun.*, vol. 13, no. 8, pp. 4369–4382, 2014.
[47] C. Saha and H. S. Dhillon, "Millimeter Wave Integrated Access and Backhaul Networks: Performance Analysis and Design Insights," *IEEE Trans. Wireless Commun.*, vol. 18, no. 12, pp. 5524–5541, 2019.
[48] T. Fukui, Y. Sakaue, K. Minami, and T. Taniguchi, "Delay-Based Shaper With Dynamic Token Bucket Algorithm for Deterministic Networks," *IEEE Access*, vol. 10, pp. 114 424–114 433, 2022.
[49] B. Rengarajan, G. Rizzo, and M. Ajmone Marsan, "Energy-optimal base station density in cellular access networks with sleep modes," *Comput. Netw.*, vol. 78, pp. 152–163, 2015.
[50] R. Deng, B. Di, H. Zhang, L. Kuang, and L. Song, "Ultra-Dense LEO Satellite Constellations: How Many LEO Satellites Do We Need?" *IEEE Trans. Wireless Commun.*, vol. 20, no. 8, pp. 4843–4857, 2021.
[51] E. Zanotto and L. Maccari, "Simulating Urban Satellite-Based Vehicular Networks: Focus on Maps, Building Heights, or Vehicle Density?" in *Proc. WONS*, 2025, pp. 1–8.
[52] M. H. Amiri, N. Mehrabi Hashjin, M. Montazeri, S. Mirjalili, and N. Khodadadi, "Hippopotamus optimization algorithm: a novel nature-inspired optimization algorithm," *Sci. Rep.*, vol. 14, no. 1, Feb. 2024.
[53] K. Haneda *et al.*, "5G 3GPP-Like Channel Models for Outdoor Urban Microcellular and Macrocellular Environments," in *Proc. IEEE VTC Spring*, 2016, pp. 1–7.
[54] H. Kim, "Enhanced Mobile Broadband Communication Systems," in *Design and Optimization for 5G Wireless Communications*. Hoboken, NJ, USA: Wiley-IEEE Press, 2020, pp. 239–302.
[55] World Population Review, "Milan Population 2023." [Online]. Available: https://worldpopulationreview.com/world-cities/milan-population
[56] N. Piovesan, D. López-Pérez, A. De Domenico, X. Geng, H. Bao, and M. Debbah, "Machine Learning and Analytical Power Consumption Models for 5G Base Stations," *IEEE Commun. Mag.*, vol. 60, no. 10, pp. 56–62, 2022.
[57] Y. Li, F. Baccelli, H. S. Dhillon, and J. G. Andrews, "Statistical modeling and probabilistic analysis of cellular networks with determinantal point processes," *IEEE Trans. Commun.*, vol. 63, no. 9, pp. 3405–3422, 2015.
[58] N. Deng, W. Zhou, and M. Haenggi, "The Ginibre Point Process as a Model for Wireless Networks With Repulsion," *IEEE Trans. Wireless Commun.*, vol. 14, no. 1, pp. 107–121, 2015.
[59] I. A. Gedel and N. I. Nwulu, "A techno-economic comparison of 5G centralized wireless network architectures," *Radioengineering*, vol. 30, no. 5, pp. 1406–1416, 2021.
[60] H. S. Dhillon and V. V. Chetlur, *The Poisson Line Cox Process*. Cham: Springer International Publishing, 2020, pp. 31–46.



Laura Finarelli received her B.Sc. and M.Sc. degrees in Mathematics from the University of Verona and the University of Parma, respectively. Her main research interests include wireless communication systems and energy-efficient networking, with a particular focus on moving infrastructures used as RAN enhancers. She is currently pursuing a Ph.D. at TU Berlin, with a double affiliation at HES-SO Valais.



Falko Dressler is a full professor and Chair for Data Communications and Networking at the School of Electrical Engineering and Computer Science, TU Berlin. Dr. Dressler has been associate editor-in-chief for IEEE Trans. on Network Science and Engineering, IEEE Trans. on Mobile Computing and Elsevier Computer Communications. He is an IEEE Fellow and an ACM Fellow. His research objectives include next generation wireless communication systems in combination with distributed machine learning and edge computing for improved resiliency.



Marco Ajmone Marsan was a Research Professor at the IMDEA Networks Institute in Spain and a Professor at the Politecnico di Torino and at the University of Milan in Italy. He is IEEE Life Fellow, member of the Academia Europæa and of the Academy of Sciences of Torino. He is qualified as "ISI Highly Cited Researcher" in computer science and listed in Stanford University World's Top 2% Scientists. He received an honorary PhD from the Budapest University of Technology and Economics.



Gianluca Rizzo is Associate Professor at Università di Torino, Italy, and Senior Research Associate at HES-SO Valais, Switzerland. He was previously with the IMDEA Networks Institute and UNIFG. He is IEEE Senior Member. His main research interests are in the design, modeling, and performance evaluation of distributed systems. He has been working on the design and evaluation of algorithms for dynamic management of wireless networks, opportunistic communication paradigms such as Floating Content, and QoS provisioning in vehicular networks.